SEDIMENTOLOGY the journal of the International Association of Sedimentologists

Sedimentology (2020) doi: 10.1111/sed.12747

Reservoir architecture and heterogeneity distribution in floodplain sandstones: Key features in outcrop, core and wireline logs

LUIS MIGUEL YESTE*, AUGUSTO N. VARELA†‡§, CÉSAR VISERAS*, NEIL D. MCDOUGALL¶ and FERNANDO GARCÍA-GARCÍA*

**Sedimentary Reservoirs Workgroup (SEDREGROUP), Department of Stratigraphy and Palaeontology, Facultad de Ciencias, S/N, 18003, University of Granada, Granada, Spain (E-mail: lmyeste@sedregroup.com)*

†Cátedra de Micromorfología de Suelos, Facultad de Ciencias Naturales y Museo, Universidad Nacional de La Plata, Calle 122 y 60 s/n (1900), La Plata, Argentina

‡Y-TEC S.A, Av. del Petróleo s/n (1923), Berisso, Argentina

§Consejo Nacional de Investigaciones Cientificas y Técnicas CONICET, Calle 8 1467, B1904 La Plata, Buenos Aires, Argentina

¶Consultant Sedimentologist & Stratigrapher, 28290, Madrid, Spain

Associate Editor – Charlie Bristow

ABSTRACT

Exploration and production from formations deposited in low-gradient fluvial systems is typically associated with a high degree of uncertainty; a reflection of the inherent characteristics of these environments, notably the dominance of non-reservoir floodplain fines, rapid lateral facies variations and associated heterogeneities at different scales. However, for a field development to be successful it becomes crucial to know the location, geometry, dimensions and connectivity of the most permeable facies, related to the main channel and the associated proximal overbank deposits (crevasse-splay complexes). With the aim of addressing this problem, a multi-disciplinary study is presented, combining outcrop data, high-resolution sedimentological descriptions and advanced visualization techniques based on Digital Outcrop Models. This is compared with subsurface data from behind the outcrop (core, gamma ray and borehole image logs). The Mudstone–Sandstone Unit of the Triassic Red Beds of Iberian Meseta formation in south-central Spain was selected for the present study. The unit is characterized by the lateral and vertical stacking of four architectural elements: (i) channelized sandstone bodies; (ii) asymmetrical sigmoidal-shaped sandstone bodies; (iii) lobe-shaped to sheet-like sandstone bodies; and (iv) sheet-like mudstones. These elements represent meandering channel, crevasse-channel-splay and floodplain sub-environments, comprising a distal, low-gradient meandering fluvial system. Together with well-documented outcrop and core facies, calibrated log responses are also presented for the channel bodies (bell-shape Gamma Ray profile, random azimuths and low to high dip angles), the crevasse-splay bodies (funnel-shape Gamma Ray profile, unidirectional azimuths and low dip angles) and the floodplain deposits (serrated Gamma Ray profile, unidirectional azimuths and very low dip angles). The full integration of outcrop and subsurface datasets has enabled generation of a robust conceptual model with predictive potential when establishing the three-dimensional stacking of facies, distribution of heterogeneities, and the connectivity between reservoir rock geobodies of primary (channel) and secondary (crevasse complex) interest in this type of fluvial reservoir.

Keywords Borehole image, crevasse-splay, gamma ray, meandering fluvial system, outcrop/behind outcrop characterization, palaeosols, TIBEM, Triassic.

INTRODUCTION

The characterization of fluvial reservoirs, and more specifically of meandering channel systems is often highly complex, due to the three-dimensional (3D) characteristics of sandstone geo-bodies, the rapid lateral facies variations and the associated heterogeneities at different scales (Jordan & Pryor, 1992; Legarreta *et al.*, 1993; Bridge, 2001; Pranter *et al.*, 2008). Accordingly, the accurate planning and optimization of recovery options in this type of hydrocarbon reservoir demands a detailed 3D knowledge of both geo-bodies and the distribution of heterogeneities (Weber, 1986; Browne & Slatt, 2002; Pranter *et al.*, 2008, 2009, 2014; Slatt *et al.*, 2011). To date, fluvial sedimentological research has tended to focus on the characterization and distribution of heterogeneities within the component sand bodies comprising the main channels (Allen, 1983; Blakey & Gubitosa, 1984; Bridge & Tye, 2000; Gouw & Berendsen, 2007; Pranter *et al.*, 2009; Jenson & Pedersen, 2010, and others). However, sedimentological research focussed on the detailed study of the overbank deposits, typical of this type of depositional environment, has been limited. In fluvial systems dominated by aggradation, fine-grained floodplain deposits and sandstone geo-bodies related to crevasse-splay processes are a key constituent in the stratigraphic succession, and in fact provide significant insights into channel stacking, avulsion mechanisms and even distances to the main channel (Mjøs *et al.*, 1993; Kraus & Aslan, 1999; Moscariello, 2009; Varela *et al.*, 2012; Burns *et al.*, 2017; Gulliford *et al.*, 2017).

To achieve an appropriately realistic 3D characterization of all the variables that generate heterogeneities in fluvial reservoirs has been a long-term challenge for many workers from both an academic and industry perspective. In order to address this challenge a substantial volume of high-quality data is required for the estimation of the dimensions and distribution of the heterogeneities in this type of fluvial reservoir.

In this sense, the study of outcrop analogues is a useful tool, which complements the sparse subsurface data and aids in constructing more realistic conceptual models (Miall, 1990; Kokureck *et al.*, 1991; Tyler & Finley, 1991; Wizevich, 1991; Yoshida *et al.*, 2001; Ajdukiewicz & Lander, 2010; Scott *et al.*, 2013; Pranter *et al.*, 2014; Franke *et al.*, 2015). If in addition to the outcrop data, subsurface data of the same examples are available, an appropriate database can be constructed in order to properly constrain the geometries and dimensions of the sandstone geo-bodies. From this, realistic models can be generated, that capture both facies at high resolution and the distribution of the heterogeneities within reservoirs. The integrated study of outcrop and subsurface data, known as Outcrop/Behind Outcrop characterization (hereinafter 'OBO') (Browne & Slatt, 2002; Slatt *et al.*, 2011; Viseras *et al.*, 2018; Yeste *et al.*, 2018) is the methodology chosen in this paper.

The aims of this paper are: (i) to present a detailed analysis of sedimentary facies, geometries and stacking patterns within fine-grained floodplain deposits and sandstone geo-bodies associated with crevasse-splay deposits in the mudstone–sandstone (M-S) Unit of TIBEM; (ii) to determine the key features necessary for the recognition and characterization in subsurface well data of these deposits; and (iii) to develop a predictive conceptual model that represents the heterogeneities in these fluvial reservoirs.

The studied example is a Triassic succession often considered as an outcrop analogue for other hydrocarbon-productive reservoirs such as the Algerian TAGI (Trias Argilo-Gréseux Inférieur; Rossi *et al.*, 2002; Dabrio *et al.*, 2005; Viseras *et al.*, 2011; Henares *et al.*, 2014, 2016a, b; Viseras *et al.*, 2018; Yeste *et al.*, 2018). For this reason, the Outcrop/Behind Outcrop workflow has been employed, integrating standard 2D high resolution outcrop data and 3D outcrop data, developed from photogrammetry, with subsurface data from behind the outcrop including cores and core descriptions, Gamma Ray logs and borehole image logs (Yeste *et al.*, 2018). The integration of different but complementary data types (i.e. surface and subsurface data) leads to better constrained reservoir models which serve to improve the quantification and correlation of

heterogeneities within this type of fluvial reservoir.

GEOLOGICAL SETTING

The extensive, sheet-like Triassic Red Beds succession of the Iberian Meseta, south-central Spain (the TIBEM of Viseras *et al.*, 2011; Henares *et al.*, 2014, 2016a,b; Viseras *et al.*, 2018; Yeste *et al.*, 2018) are continental deposits which accumulated during the Tethyan rifting process (Late Permian–Upper Triassic; Sánchez-Moya *et al.*, 2004). The study area, located to the east of Alcaraz village (Albacete Province; Fig. 1), corresponds to the most distal part of the TIBEM outcrop as suggested by palaeocurrent data (Fernández & Dabrio, 1985; Henares *et al.*, 2014). The Triassic Red Beds succession of the TIBEM in the study area thus comprises fluvial to coastal deposits within a linked stratigraphic framework.

In the study area, the *ca* 160 m thick sedimentary succession (Ladinian–Norian) is divided into four sequences, on the basis of the predominant lithology and depositional environments (Fig. 2; Yeste *et al.*, 2018). From base to top, they are: (i) a mudstone–sandstone unit (M-S Unit), that includes both a meandering channel system and overbank sandstone deposits embedded in distal floodplain mudstones; (ii) a sandstone unit (S Unit) corresponding to a braided system; (iii) a heterolithic unit (H Unit) comprising alternating sandstone and mudstone layers deposited in a fluvial–tidal transition zone; and (iv) a mudstone–evaporitic unit (M-E Unit) composed of silt-rich coastal plain facies and intertidal sabkha evaporites. The suggested sub-division groups and simplifies the previous divisions proposed by Fernández & Dabrio (1985) (Sequences I to IV) and Arche & López-Gómez (2014), which divided the succession on the basis of the classic Germanic Trias Units, Keuper (K1 to K5). The deposits described in this paper correspond to a 90 m thick heterolithic section of mudstone and sandstone, the M-S Unit (Yeste *et al.*, 2018; Fig. 2) or Sequence II of Fernández & Dabrio (1985) and Unit K1 of Arche & López-Gómez (2014).

METHODOLOGY AND DATA DISTRIBUTION

The OBO characterization workflow applied in this study is multi-disciplinary, including detailed sedimentological description from both surface (outcrop-derived and digital outcrop-derived observations and measurements) and subsurface (cores and well logging) sources (Fig. 3).

In order to study the geometry, internal structure, sequence trends and spatial relationship between the main architectural elements, a total of 0.813 km^2 of outcrop has been studied. For the characterization of lateral facies variability, a total of 18 sedimentological logs have been constructed (Fig. 1). From the principal architectural element, or the Main Channel, in the outcrop, (CP-0, Fig. 1), eight sedimentological logs were completed towards the eastern margin (CPMR1 to CPMR8, Fig. 1) and nine towards the western margin (CPML1 to CPML9; Fig. 1). The lateral variability of facies was also observed in another channel complex to the north, characterized by an additional two sedimentological logs (CBML1 and CBML2) although these have not been fully included in all aspects of the study. In addition to the 18 partial sections listed above, and to fully characterize the vertical variability of facies, a complete sedimentological log was constructed through a section of 72 m (PVN1, Fig. 1) in the M-S Unit.

Digital Outcrop Models (DOM) have also been created from photogrammetry with an RPAS (Remotely Piloted Aircraft System) to complete the outcrop-derived measurement dataset (Fig. 3). The RPAS used was a multi-rotor octocopter with a Sony ILCE 5000 camera of 20 Mpx (Sony, Tokyo, Japan). The image acquisition strategy required two types of flight along the outcrop: (i) a flight plan at 50 m height with the camera oriented at 90 degrees (perpendicular to the ground surface); and (ii) a flight plan at different heights (depending on the zone of the outcrop) with the camera oriented at 0 degrees (perpendicular to the outcrop). The average Ground Sampling Distance (GSD) was 1.32 cm. The total covered area spans over 0.813 km^2. For the DOM, the professional software Agisoft Photoscan^{TM} was used, which was specifically designed for drone-based mapping.

In the studied example, two slim-hole [6.25″ (*ca* 14 cm) diameter], behind-outcrop wells allowed subsurface characterization of the key facies. (Fig. 1): (i) Well S2P4, located at the top of the studied succession (M-S Unit), has a section of 70 m and; (ii) Well K2P1 located at the top of the S Unit (see Fig. 2) drilled to a depth of 42 m; of which the uppermost 22 m correspond to the S Unit and the remaining 20 m to

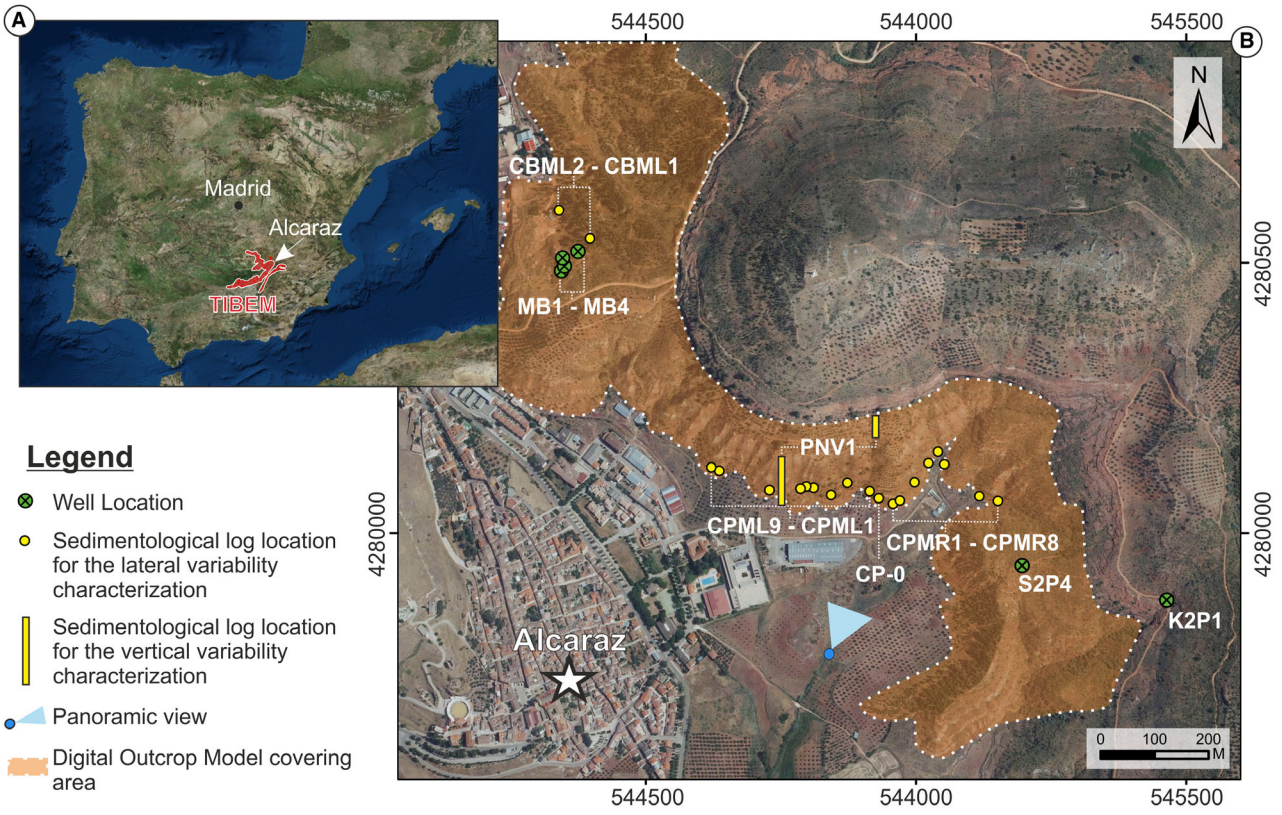

Fig. 1. (A) Location of the study area (Alcaraz village, Albacete province, Spain). (B) Close-up view of the location of the studied outcrops. The orange shading represents the outcropping study area and the area covered by Digital Outcrop Models (DOM). Yellow points and yellow rectangles represent the location of sedimentological logs constructed to enable the characterization of lateral and vertical variability, respectively. Green points are well locations. Acronyms correspond to the names of profiles and wells, as explained in the text.

the studied unit (M-S Unit). The distance between Wells S2P4 and K2P1 is 275 m. Both wells were drilled with continuous core recovery and wireline log data was obtained. Core slabbing was subsequently carried out in order to enhance the visibility of sedimentary features on the core surface and allow the identification of the main simple lithofacies classes (Table 1). Well log data include the Gamma Ray log (GR) in addition to borehole imaging from Optical and Acoustic Televiewers (OBI and ABI, respectively). The ABI is a slim-hole logging tool with an ultrasonic transducer sensor. This tool provides a 360° oriented acoustic image (amplitude and travel time). The OBI is a slim-hole logging tool with high sensitivity digital image sensor. This tool provides a 360° RGB true colour-oriented image. Dip tadpoles, together with GR pattern analyses, provide information on the spatial distribution, orientation and dip of the main sedimentary surfaces and structures. Supplementary dip information is also included from four additional wells (MB1 to MB4) described in detail in Viseras *et al.* (2018).

OUTCROP, CORE AND WIRELINE LOG CHARACTERISTICS OF FACIES ASSOCIATIONS

Ten facies associations (FA) from the TIBEM were identified (Fig. 4; Table 1). The following section contains a detailed description of each facies association including lateral and vertical lithofacies variation, geometric data, bounding surfaces and the dimensions of the sedimentary bodies, as described both in outcrop and subsurface (core, GR log response and image logs), in order to characterize the spatial distribution of heterogeneities. Gamma-ray log patterns (electrofacies patterns) were interpreted according to the models of Emery & Myers (1996) and Slatt (2013).

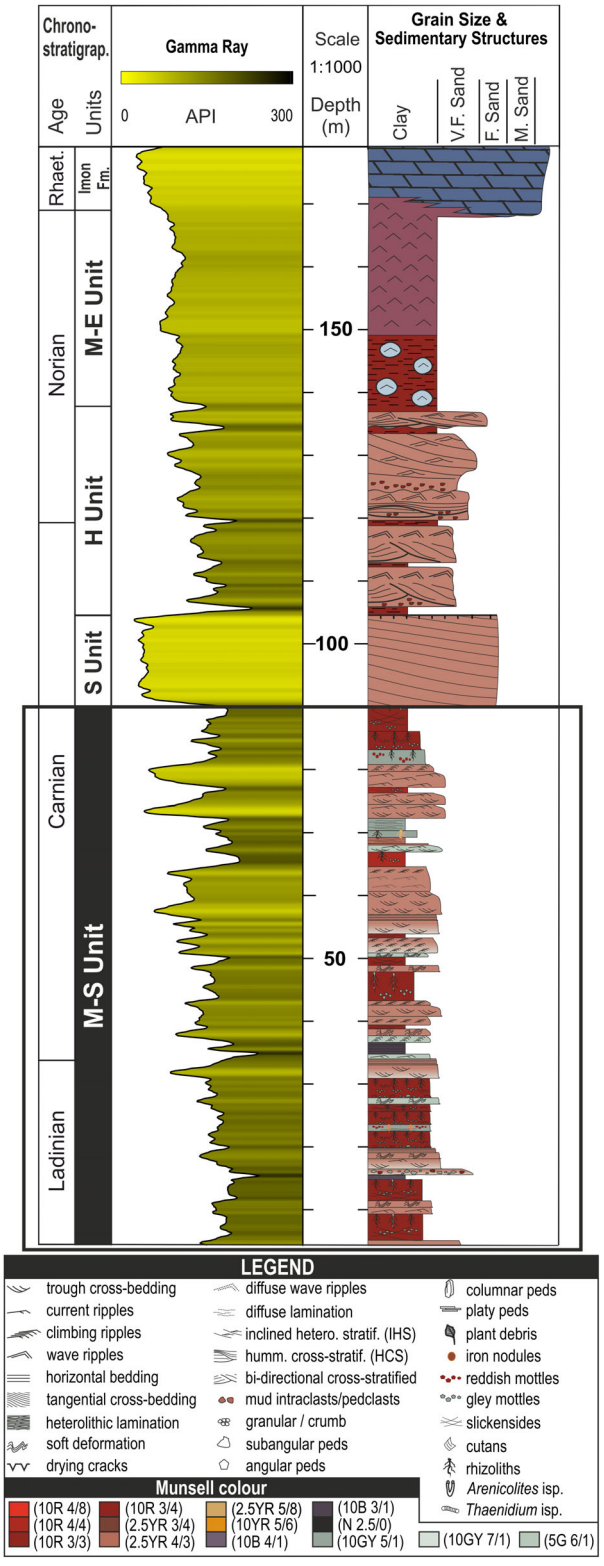

Fig. 2. Simplified Triassic Red Beds of Iberian Meseta (TIBEM) stratigraphic and lithological succession in the Alcaraz area based on the Gamma Ray log. The black square highlights the studied interval (Mudstone–Sandstone Unit) in the general stratigraphic succession. M-S Unit: Mudstone–Sandstone Unit; S Unit: Sandstone Unit; H Unit: Heterolithic Unit; M-E Unit: Mudstone–Evaporitic Unit.

Facies Association 1: Main channel

Description

Facies Association 1 (FA 1) comprises a fining-upward sequence ranging from conglomerates, characterized by the presence of mudstone rip-up clasts, to very fine-grained sandstones (Fig. 4A). FA 1 occurs as lenticular-shaped bodies up to 3 m thick with a lateral extension of up to 30 m perpendicular to the main flow direction. These lenticular bodies show concave-up erosive bases, whilst the tops are horizontal and sharp (Tables 1 and 2; and Fig. 4A). Internally they comprise conglomerates, with pebbly mudstone (Gm) as basal lags. Overlying the basal lags are medium to fine-grained sandstones with planar to trough cross-bedding (St) and very fine-grained sandstone with current ripples (Sr) towards the top (Table 1). Sometimes packages of FA 1 also show a final interval of laminated fine-grained deposits (Fl). Typically, the tops of FA 1 bodies are characterized by *Arenicolites* isp. and less frequently *Taenidium* isp. trace fossils (Table 2; Fig. 4A).

The GR log through FA 1 typically comprises several packages with an initial decrease in API values followed by repeated increases and decreases in API values on a decimetre to metre scale (Fig. 4A). The OBI and ABI logs show a high intensity and high amplitude contrast at the base of this FA. Internally these image logs are characterized by common sine wave surfaces (interpreted as cross-bed foresets) and towards the top display a speckled to massive appearance with few non-sine wave surfaces (Fig. 4A).

Interpretation

This fining-upward succession, together with the lenticular geometries and erosive lower surfaces suggest that FA 1 should be interpreted as the deposits of a main channel. Within this framework; the vertical lithofacies variation (Gm–St–Sr), described above, indicates decreasing flow energy (Table 1). The occasional presence of laminated fine-grained deposits (Lithofacies Fl) is interpreted as a mud plug due to neck cut-off of a meandering channel (Viseras *et al.*, 2018). In contrast, the common occurrence of *Arenicolites* tubes unconnected with any fine-grained deposits suggests an abrupt avulsion of the fluvial system (Hubbard *et al.*, 2011; Durkin *et al.*, 2017). The non-typical GR profile of FA 1, a coarsening-

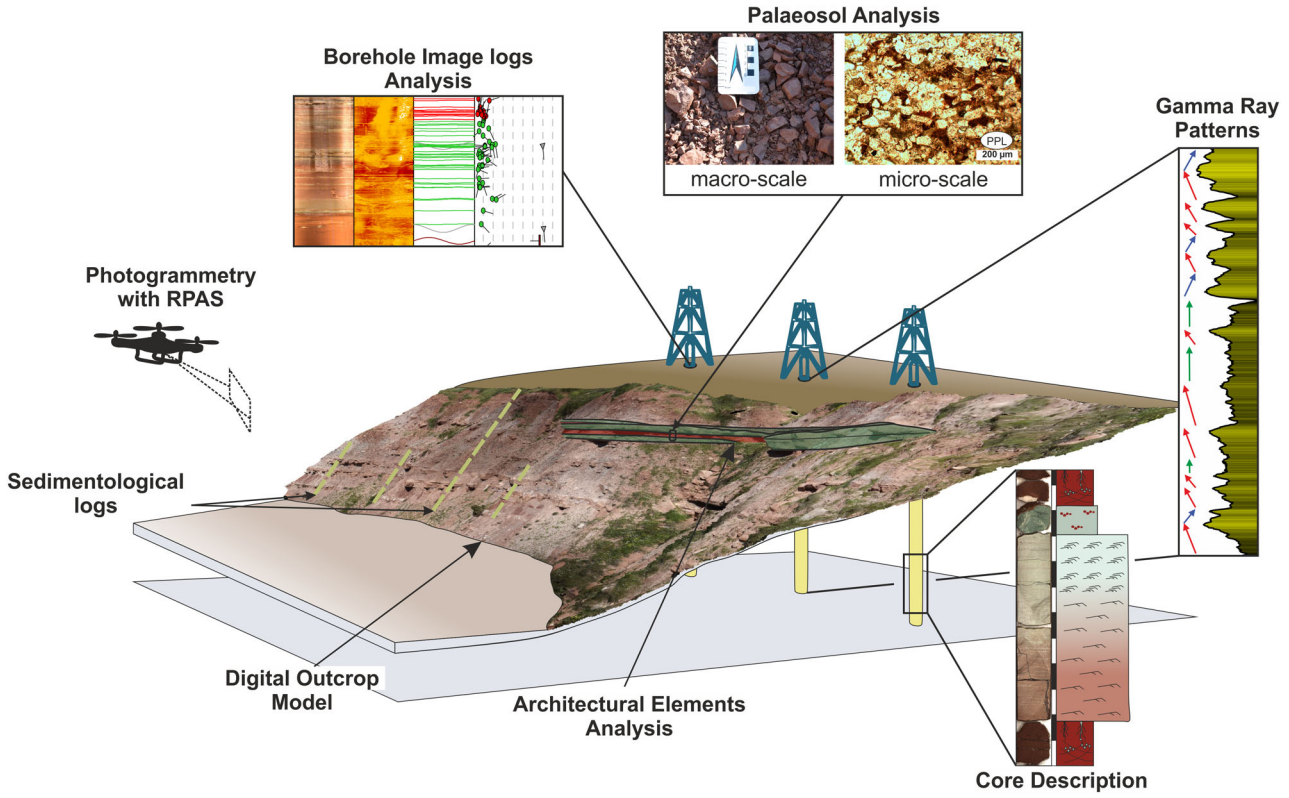

Fig. 3. Outcrop/Below Outcrop (OBO) characterization workflow designed and applied in this study including outcrop-derived and digital outcrop-derived observations and measurements, core description, Gamma Ray logging, borehole imaging and palaeosol analysis. RPAS: Remotely Piloted Aircraft System.

upward trend (funnel shape) at the base and fining-upward (bell shape) towards the top, most likely reflects the occurrence of mudstone rip-up clast conglomerates as basal lags (Selley, 2004; Henares *et al.*, 2016a,b; Viseras *et al.*, 2018). The high intensity and amplitude contrast at the base of the facies package, in both OBI and ABI logs, is interpreted to record the main channel erosive surface. Above this surface, the presence of sine wave surfaces in OBI and ABI logs corresponds to cross-stratified sandstone (correlated to the cross-stratified sandstones observed in outcrop), whereas the speckled to massive final interval without sine wave surfaces is interpreted as current rippled sandstones (Keeton *et al.*, 2015).

Facies Association 2: Point bar

Description

Facies Association 2 (FA 2) is characterized by a fining-upward facies sequence passing from mudstone rip-up clast conglomerate to very fine-grained sandstones (Fig. 4B). Outcrop data indicates that FA 2 occurs as asymmetrical, sigmoidal-shaped bodies, up to 3.6 m thick and with lateral extensions of up to 100 m. These bodies are typically bounded by horizontal and erosive bases, whilst the tops are horizontal and sharp (Tables 1 and 2; Fig. 4B). FA 2 is easily recognized, in outcrop by the occurrence of several inclined master bedding surfaces perpendicular to the palaeocurrent direction, typically showing an upward increase in dip angle. Internally, FA 2 comprises sets of trough cross-bedding (St) and current ripples (Sr) towards the top of the facies sequence (Table 1). Locally, mud drapes occur between the inclined master surfaces, both as layers within the packages and as drapes over the inclined master surfaces. In addition, the top of the FA 2 package shows evidence of wave reworking (Sw) and contains both *Arenicolites* isp. and *Taenidium* isp. trace fossils (Table 2; Fig. 4B). The inclined master surfaces, first recognized in outcrop, are recognized in core as inclined erosive surfaces commonly draped by thin claystone layers (Fig. 4B).

The FA 2 GR log typically shows a decrease in API values above the base and continues with

Table 1. Lithofacies identified in the Mudstone–Sandstone (M-S) Unit. See Fig. 4 for photographic examples of each lithofacies.

Code	Texture and fabric	Sedimentary structures and characteristics	Main process
Gp	Pebble-cobble. Clast or matrix-supported	Massive, weak horizontal bedding or planar cross-bedding. Erosive base and mud rip-up clasts	High energy traction current
Sm	Fine to medium sand	Massive. Rare presence of mud clasts	Channel fill due to waning flow
Sh	Fine to medium sand	Horizontal lamination	Sheet flow. Upper flow regime
St	Fine to medium sand	Trough cross-bedding. Sometimes, mud chips lining the cross-beds	Migration of megaripples and dunes. Channel fill
Sp	Very fine to medium sand	Planar cross-bedding	Megaripple migration
Sr	Very fine to fine sand	Current ripple lamination	Migration of current ripples
Sc	Very fine to fine sand	Asymmetrical climbing ripple lamination	Combination of traction and settling from suspension
Sw	Very fine sand	Wave ripple lamination	Oscillatory flow in a standing body of water
Sd	Very fine sand	Convolute lamination. Dish plate structure. Soft-sediment deformation structures	Deposition from flow and unstable water-saturated substrate
Sl	Very fine sand	Diffuse horizontal lamination or diffuse current ripple	Settling from suspension or migration of current ripples. Diffuse structures due to soil development
Sb	Very fine to medium sand	Massive. Presence of rhizoliths, *Arenicolites* isp. and *Taenidium* isp.	Structureless due to bioturbation
Lm	Silt	Massive. Abundant rhizoliths	Soil develops on former overbank fines
Lr	Silt	Current ripple lamination. Sometimes, wave ripple lamination	Migration of current ripples
Ll	Silt	Horizontal lamination. Uneven lamination	Settling from suspension. Lower flow regime
Fm	Clay.	Slickenside, wedge shape peds, angular and subangular blocky peds, cutans, motts and rhizoliths	Soil develop on former overbank fines
Fl	Clay	Horizontal lamination (lower flow regime). Uneven lamination. Sometimes, presence of plant remains and coal	Settling from suspension
Htf	Very fine to silt and clay	Heterolithic bedding. Flaser, wavy and/or linsen lamination	Settling from suspension alternating with tractive episodes
Cm	Limestone	Massive micritic mudstones	Settling from suspension

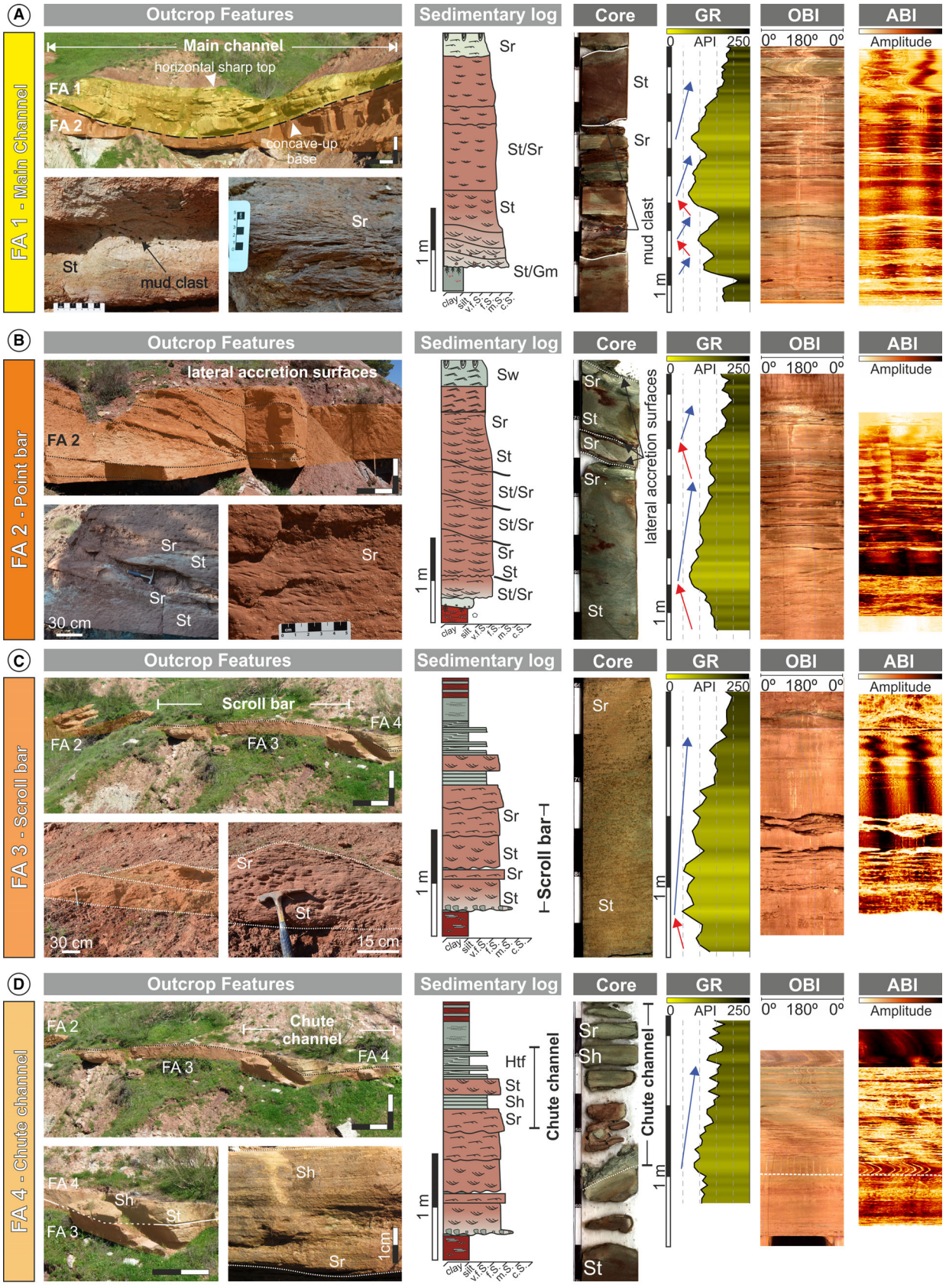

Fig. 4. For caption, see page 10.

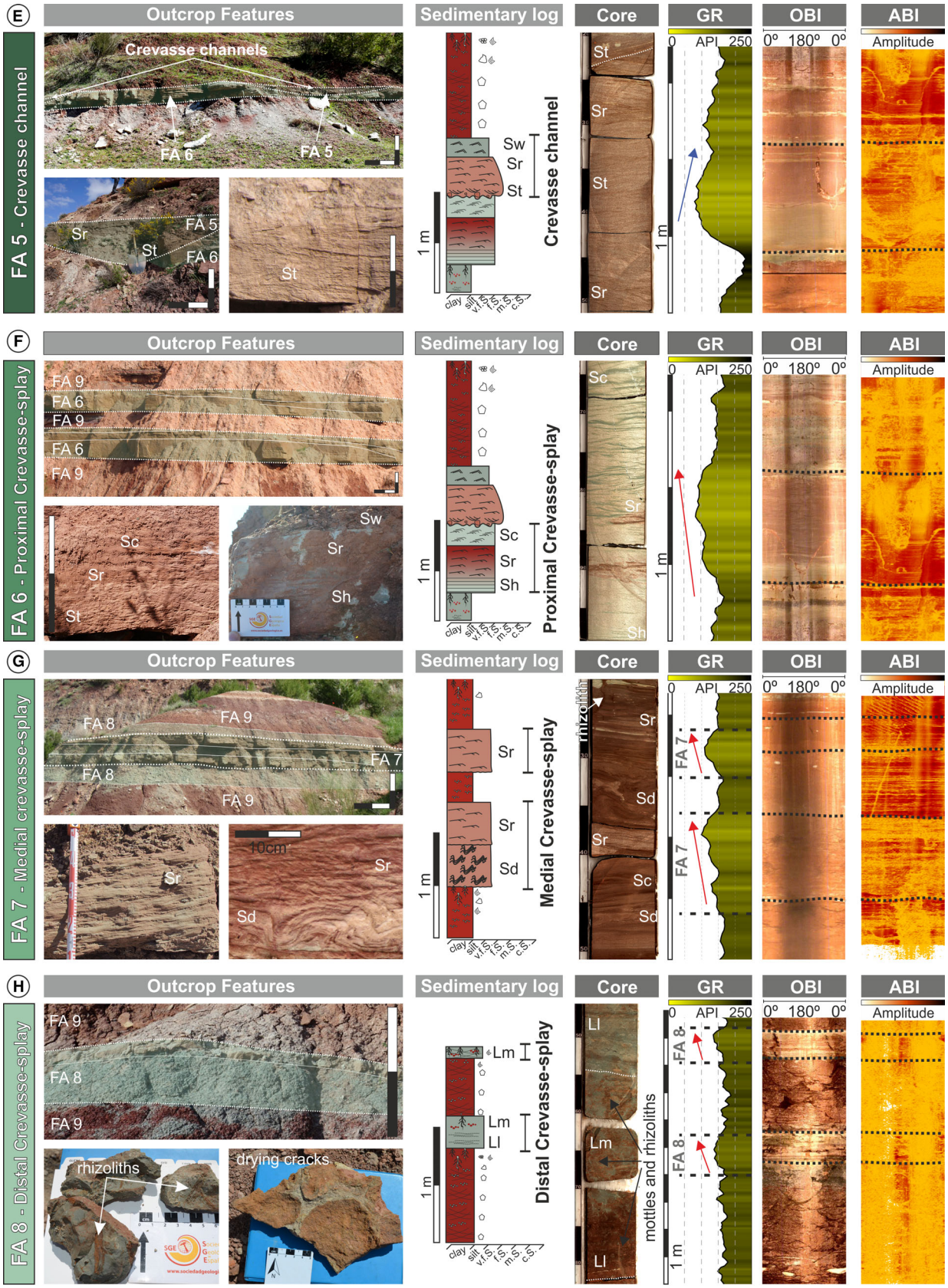

Fig. 4. Continued

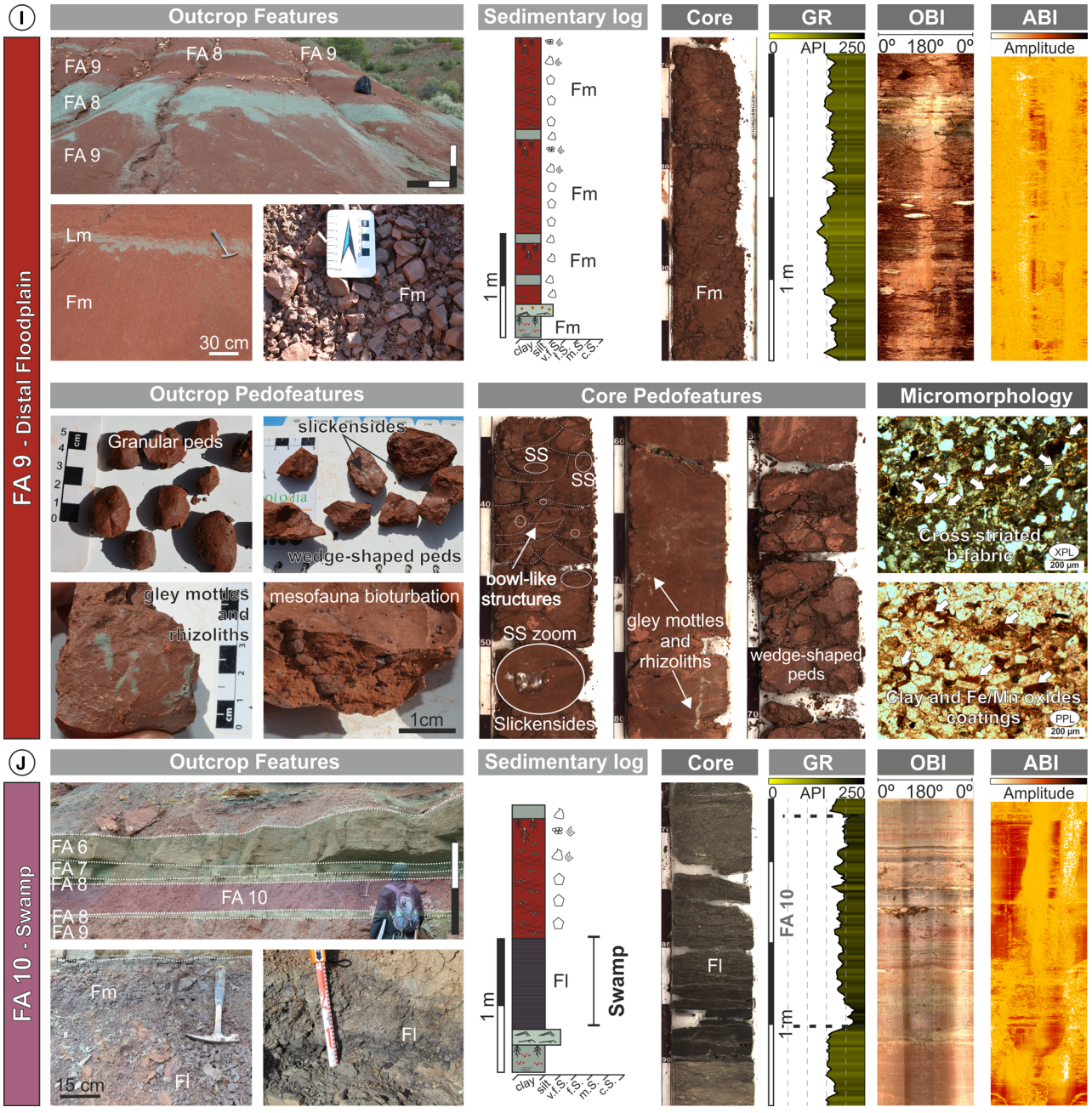

Fig. 4. Characteristics in outcrop, sedimentary log, core, gamma ray log and borehole images (GR – Gamma Ray; OBI – Optical Televiewer; ABI – Acoustic Televiewer) features for each facies association identified. (A) to (J) show outcrop and behind outcrop characteristics for Facies Associations 1 to 10, main channel, point bar, scroll bar, crevasse channel, proximal crevasse-splay, medial crevasse-splay, distal crevasse-splay, distal floodplain and swamp deposits, respectively. Hammer for scale is 28 cm long.

an increase in API values towards the top (Fig. 4B). The OBI and ABI logs also show several inclined master surfaces distinguished by high intensities and contrasts in amplitude. Between these surfaces, sine waves are typically overlain by massive to speckled intervals.

Interpretation

These asymmetrical sigmoidal geometries, observed in outcrop, together with the characteristic occurrence of several inclined surfaces perpendicular to the palaeocurrent and the fining-upward succession suggest point bar deposits. The inclined

Table 2. Summary of facies associations identified in the Mudstone–Sandstone (M-S) Unit. See text for details. See Table 1 for lithofacies description. See Fig. 4 for photographic examples of each facies association (FA).

FA	Lithofacies	Description	Geometry	Boundary surfaces (L = lower; U = upper)	Thickness	Width	Environmental interpretation
1	Gp, St, Sr, Sm, Fl	Mudstone rip-up clasts. Trough cross-bed sets of 20 × 6 cm. Shows *Arenicolites* isp. and *Taenidium* isp. at the top	Lenticular	L: Concave-up and erosive U: Horizontal and sharp	Up to 3.0 m	Up to 30 m perpendicular to the main flow direction	Main channel
2	Gp, St, Sp, Sr, Sc, Sw, Sb, Sd, Sm, Lr, Ll	Mudstone rip-up clasts. Lateral accretion surfaces increasing dip towards the top (5–20°). Internally composed of trough cross-bed sets of 27 × 9 cm and counter-current ripples towards the top. Sometimes shows mud drapes or mud laminae between lateral accretion surfaces. Shows *Arenicolites* isp. and *Taenidium* isp. at the top	Asymmetrical sigmoidal	L: Horizontal and erosive U: Horizontal and sharp	Up to 3.6 m	Up to 100 m	Lower and middle point Bar
3	Sr, St, Sp, Sh, Sm	Mudstone rip-up clasts. Trough cross-bed sets. Current ripples towards the top	Asymmetrical sigmoidal	L: Horizontal and erosive U: Horizontal and undulated	Up to 1.5 m	Up to 30 m	Scroll bar
4	Sr, Sh, St, Htf	Alternation between Sr/St from low flow regime with Sh in high flow regime. Towards the top shows Htf as final stage filling	Lenticular	L: Concave-up and erosive U: Horizontal and sharp	0.7–0.8 m	Up to 3 m	Chute channel
5	St, Sr, Sw	Mudstone rip-up clasts at the base. Show trough cross-bed sets of 25 × 2 cm and current ripples. Sometimes towards the top shows Lithofacies Sw	Lenticular	L: Concave-up and erosive U: Horizontal and sharp	0.4–1.1 m	Up to 6 m	Crevasse channel
6	Sh, Sr, Sc, Sd	The vertical stacking of facies shows the transition from Sh to Sr/St, finally climbing ripple and syn-sedimentary deformation towards the top	Lobe	L: Horizontal and sharp U: Convex-up and sharp	Up to 2.0 m	Up to 130 m	Proximal crevasse-splay complex

Table 2. (continued)

FA	Lithofacies	Description	Geometry	Boundary surfaces (L = lower; U = upper)	Thickness	Width	Environmental interpretation
7	Sr/Sc, Sm, Sl, Sw, Sd	Climbing ripple and current ripple at the base. Alternating with syn-sedimentary deformation. At the top rootlets. Desiccation cracks	Lobe	L: Horizontal and sharp U: Convex-up and sharp	Up to 1.5 m	Up to 70 m	Medial crevasse-splay complex
8	Fm, Lm, Ll, Fl, Sl	Lower flow regime lamination and palaeosol development to the top (rootlets, mottles and cutans). Desiccation cracks. Sometimes shows *Arenicolites* isp. at the top	Lobe to tabular	L: Horizontal and sharp U: Convex-up and sharp	Up to 0.8 m	Up to 30 m	Distal crevasse-splay complex
9	Fm	Slickensides, wedge-shape peds, angular and subangular blocky peds, cutans, bowl-like structures, Gilgai microrelief, motts and rhizoliths	Tabular	L and U: Horizontal and sharp	From cm to 10 m	100–1000 m	Distal floodplain
10	Fl, Fm, Cm	Gley dark purple to dark grey colour mudstone. Usually laminated. Desiccation cracks. Sporadic massive micritic limestone laminae	Tabular	L and U: Horizontal and sharp	From cm to 2 m	100 m	Swamp

surfaces with increasing dip angle are thus interpreted as lateral accretion surfaces. The presence of current ripples flowing up-slope along these accretion surfaces (i.e. perpendicular to the palaeoflow), are interpreted as the result of the helicoidal flow developed in the meander band (Viseras *et al.*, 2018). The occurrence of mud drapes between the lateral accretion surfaces represents deposition during a waning flood stage (Thomas *et al.*, 1987; Viseras *et al.*, 2018). The presence of Lithofacies Sw and *Arenicolites* tubes could indicate periods of ponding and wave reworking. The basal coarsening-upward (funnel shape) interval in the GR log would correspond to the presence of mudstone rip-up clasts (Selley, 2004; Viseras *et al.*, 2018). The high contrast surfaces, seen in the image logs, represent each lateral accretion surface, whereas internal deposits of each lateral accretion package are represented by lithofacies St (sine wave surfaces) and Sr (speckled to massive intervals).

Facies Association 3: Scroll bar

Description

Facies Association 3 (FA 3) is similar in some respects to FA 2 although the dimensions and thickness of the packages are somewhat reduced. It is characterized by a fining-upward sequence passing from mudstone rip-up clast conglomerate (Gm) into very fine-grained sandstones. (Fig. 4C). FA 3 typically occurs as asymmetrical sigmoidal-shaped bodies which are up to 1.5 m thick and up to 30 m in lateral extent. These bodies show horizontal and erosive bases, whilst the top surfaces are horizontal and undulated (Tables 1 and 2; Fig. 4C). This facies association mainly comprises sets of trough cross-bedding (St), locally with mudstone rip-up clasts lining the set base and typically associated, in wells behind the outcrop, with notably higher Gamma Ray API values. Towards the top of the facies package, current ripples (Sr) are dominant. In core, this facies sequence of trough cross-bedding with local rip-up clast lags overlain by current ripples, is easily distinguished.

The GR log through FA 3 typically shows an increase in API values towards the top (Fig. 4C). The OBI and ABI image logs show a generally speckled appearance with sine curves at the base. Towards the top, sets of continuous sine curves, bounded by scour surfaces, can also be recognized. In the ABI log, the speckling is bright and sets of continuous sine curves are dark coloured.

Interpretation

Facies Association 3 is characterized by thin, convex-up (undulatory tops) asymmetrical–sigmoidal packages with a fining-upward facies succession, all of which can be interpreted in terms of scroll bar deposits (Nanson & Page, 1983). The undulated tops, as observed, in outcrop together with the reduced dimensions, the absence of mud drapes, the presence of rip-up clasts only at the base, and the prevalence of current ripples in core characterize this facies association in contrast to FA 2. The presence of sets of trough cross-bedding, with rip-up clasts lining set bases overlain by current ripples, suggests lateral migration of the scroll bars. In the image logs, the speckled appearance with sine curves reflects trough cross-bedding with mudstone rip-up clasts (Lai *et al.*, 2018). Sets of continuous sine curves, bounded by scour surfaces, correspond to different lateral accretion units within the scroll bar. The continuous sine curves represent trough cross-bedding and current ripples (Lai *et al.*, 2018).

Facies Association 4: Chute channel

Description

Facies Association 4 (FA 4) is defined by a fining-upward sequence, from fine-grained sandstones into siltstones (Fig. 4D). In outcrop, FA 4 forms lenticular bodies up to 0.8 m thick with a lateral extension of up to 3 m. Internally, this facies association is characterized by an alternation between trough cross-bedding (St) and/or current ripples (Sr) and horizontal lamination (Sh). Towards the top of the facies sequence, heterolithic flaser bedding (Htf) also typically occurs. Geo-bodies defined as FA 4 in outcrop are characterized by concave-up and erosive bases cutting down into FA3, whilst the top surfaces are both horizontal and sharp (Tables 1 and 2; Fig. 4D). The base is distinguished in the cores as an inclined erosive surface overlain by horizontal lamination (Sh) and current rippled (Sr) or, less commonly, small-scale trough cross-bedded (St) sandstones (Fig. 4D).

Facies Association 4 is characterized by an increase in API values towards the top of the GR profile (Fig. 4D). The OBI and ABI logs are characterized by poorly developed sine waves and a high contrast scour surface at the base. The uppermost part of the package is, in contrast, characterized by a homogeneous or structureless appearance.

Interpretation

This facies association is interpreted as a chute channel, on the basis of a fining-upward trend, geo-body dimensions, a lenticular geometry and its relationship with FA 3. The horizontal laminated (Sh) and current rippled (Sr) sandstones represent deposition during higher flood stages (Nemec & Postma, 1993; Miall, 1996; Ghinassi, 2011). During this phase, the water overtops the point bar, scouring the chute channels (Briant, 1983; Ghinassi, 2011). The heterolithic flaser-bedded siltstones (Htf), in contrast, represent deposition during the receding flood stages (McGowen & Garner, 1970; Brierley, 1991; Ghinassi, 2011; Table 1). Within this framework, the gradual increase in GR values (bell shape) almost certainly records the fining-upward sequence seen in core and outcrop, from horizontal and current rippled sandstones to heterolithic flaser-bedded siltstones (Htf). It is also probable that those image log intervals characterized by poor sine waves represent horizontal laminated and current rippled sandstones, whereas the homogeneous, massive intervals correspond to the heterolithic flaser-bedded siltstones (Lai *et al.*, 2018). The scour surface seen in the image logs (see Fig. 4D) is also clearly the erosive base of the chute channel observed in outcrop.

Facies Association 5: Crevasse channel

Description

Facies association 5 (FA 5) is characterized by a fining-upward sequence passing from mudstone rip-up clast conglomerates to very fine-grained sandstones (Fig. 4E). In outcrop, FA 5 is observed to form lenticular bodies up to 1.1 m thick with a lateral extension of up to 6 m perpendicular to the main flow direction. These lenticular bodies are characterized by concave-up, erosive bases, whilst the tops are horizontal and sharp (Tables 1 and 2; Fig. 4E). FA 5 truncates the underlying strata typically assigned to FA 6 and/or FA 7. Rarely, this facies association also truncates the mud prone FA 9. Internally, FA 5 packages show thin mudstone rip-up clast conglomerates as basal lags overlain by fine to very fine-grained sandstone with trough cross-bedding (St) and very fine-grained sandstone with current ripples (Sr). Locally, towards the top, very fine-grained sandstone with oscillation ripples (Sw) also occur. In core, this association, is also characterized by the alternation of trough cross-bedded and current rippled sandstones (Fig. 4E).

The GR log is characterized by an increase in API values towards the top and a sharp base (Fig. 4E). The OBI and ABI logs show bright colours and sine waves at the base. Towards the top of the package the image logs are also characterized by thin (<10 cm), alternating bright and dark bands (bright yellow and dark brown bands in ABI log) with well-developed sine waves (Fig. 4E).

Interpretation

The fining-upward succession, together with the distinctive lenticular geometries and erosive lower surfaces strongly suggest deposition as a crevasse channel. The vertical lithofacies variation (St–Sr–Sw) and fining-upward trend (bell shape) of the GR log indicate gradual flow deceleration and overfilling of crevasse channels (Bristow *et al.*, 1999; Burns *et al.*, 2017; Table 1). Sine waves observed in OBI and ABI logs are interpreted as trough cross-bedded (St) and current rippled sandstones (St) (Lai *et al.*, 2018). The alternation of bright and dark bands (bright orange and dark brown bands in ABI log) with sine waves are likewise interpreted as very fine-grained sandstone with current ripples or oscillation ripples (bright yellow) whilst the dark brown colours likely represent mudstone layers (Donselaar & Schmidt, 2005; Xu *et al.*, 2009; Lai *et al.*, 2018).

Facies Association 6: Proximal crevasse-splay complex

Description

Facies Association 6 (FA 6) is composed of relatively thin, fine-grained sandstones (Fig. 4F). FA 6 occurs in outcrop as lobe-shape bodies, up to 2 m thick and up to 130 m in lateral extent, perpendicular to the main flow direction. These lobate bodies are characterized by a horizontal, sharp base, whilst the tops are convex-up and sharp (Tables 1 and 2; Fig. 4F). The vertical stacking of facies, whether in outcrop or core, shows a transition from horizontal laminated sandstones (Sh) to trough cross-bedded sandstones (St) and/or current rippled sandstone (Sr). Towards the top of FA 6 packages, climbing ripple cross-laminated sandstones (Sc) are also recognized.

The GR log, in contrast to most facies sequences in the studied section, shows a decrease in API values and a sharp top (Fig. 4F). The OBI and ABI logs show a set of continuous sine waves, overlying a sharp to truncated basal surface (Fig. 4F).

Interpretation

These lobate bodies with fine-grained sandstones are interpreted as the deposits of a proximal crevasse-splay complex. The vertical stacking of facies suggests variation in flood energy during deposition (Burns *et al.*, 2017). The horizontal laminated sandstones (Sh) indicate upper flow regime conditions during splay flood events. The overlying lithofacies St and/or Sr suggest a subsequent reduction in flow energy (Bristow *et al.,* 1999; Table 1). The presence of Facies Sc towards the top of the package suggests significant deposition from suspension during flow deceleration in flood splay events. The coarsening-upward trend (funnel shape) of GR logs is typical of prograding crevasse-splay lobes (Emery & Myers, 1996; Cant, 2002). Continuous sine waves interpreted in OBI and ABI logs correspond to horizontal laminated sandstones (Sh), trough cross-bedded sandstones (St) and/or current rippled sandstones (Sr) (Xu *et al.*, 2009; Keeton *et al.*, 2015; Lai *et al.*, 2018).

Facies Association 7: Medial crevasse-splay complex

Description

Facies Association 7 (FA 7) is defined as a package of thin bedded, very fine-grained sandstones typically occurring as lobe-shaped bodies up to 1.5 m thick and 70 m in lateral extent. These bodies show horizontal, sharp bases, whilst the tops are convex-up and sharp (Tables 1 and 2; Fig. 4G). This facies association comprises climbing ripples (Sc) and/or current rippled sandstones (Sr) at the base alternating with syn-sedimentary deformed sandstones (Sd). Locally, towards the top, this facies association also shows root and desiccation cracks.

The GR log is characterized by a decrease in API values with a sharp top (Fig. 4G). The OBI and ABI logs show both continuous and discontinuous sine waves. The base is represented by a sharp to truncated surface (Fig. 4G).

Interpretation

This facies association is interpreted as a medial crevasse-splay complex, on the basis of facies context, the very fine sand grain size, the presence of syn-sedimentary deformation (Sd) and current rippled sandstones (Sr) (Burns *et al.*, 2017). The occurrence of syn-sedimentary deformation (Fig. 4G) reflects rapid sediment accumulation onto a water-saturated substrate (Rossetti & Santos, 2003; Owen & Santos, 2014; Burns *et al.*, 2017; Table 1). The coarsening-upward trend (funnel shape) of the GR log is typical of prograding crevasse-splay lobes (Emery & Myers, 1996; Cant, 2002). Continuous sine wave curves, interpreted in OBI and ABI logs, correspond to current ripple cross-lamination whereas the discontinuous sine waves correspond to syn-sedimentary deformation (Xu *et al.*, 2009; Keeton *et al.*, 2015; Lai *et al.*, 2018).

Facies Association 8: Distal crevasse-splay complex

Description

Facies Association 8 (FA 8) occurs as thin, fine-grained beds, interbedded with the mudstones of FA 9. Facies package geometries are lobate to tabular, characterized by horizontal and sharp bases and gently convex-up, sharp tops. They reach up to 0.8 m in thickness and up to 30 m in lateral extent. This facies association comprises laminated siltstones and subordinate, very fine-grained sandstones. Planar laminated siltstones (Ll) are overlain by massive and diffuse laminated siltstones and mudstones with pedogenic features (rhizoliths, mottles and cutans) and also desiccation cracks (Lm). Less frequently, *Arenicolites* isp tubes occur (Tables 1 and 2; Fig. 4H). The key macromorphological features are reddish to yellowish rhizoliths (colours 10R 4/8 to 2.5YR 3-5/8), reddish and little brown mottles (colours 10R 4/4 and 2.5YR 3/4) and scar cutans. Slickensides sometimes also occur locally (Fig. 4H). FA 8 is also characterized by A/C-type palaeosol profiles.

Even though facies packages are thin, each thin FA 8 GR log shows a smooth decrease in API values and a sharp top (Fig. 4H). The OBI and ABI logs show thin high contrast bedsets, characterized by horizontal and parallel surfaces, although the OBI response is not very clear in terms of internal characteristics (Fig. 4H).

Interpretation

This facies association is interpreted as a distal crevasse-splay complex, on the basis of the very fine-grained, silt-dominated lithology, the presence of both planar and diffuse lamination as the only sedimentary structures, together with the thin, lobate to tabular geometries (Pizzuto, 1987; Mjøs *et al.*, 1993; Bristow *et al.*, 1999; Burns *et al.*, 2017). The presence of rhizoliths, mottles and cutans, coupled with the poorly developed

and often diffuse lamination suggests phases of palaeosol formation. These palaeosols should be classified as modern Entisols (Soil Survey Staff, 1998). The coarsening-upward trend (funnel shape), characteristic of the GR log is typical of prograding crevasse-splay lobes (Emery & Myers, 1996; Cant, 2002) but given the other distinguishing features, FA 8 clearly represents a distal example of such a complex. Amalgamated coarsening-upward packages suggest multiple, periodic flooding events (i.e. crevasse-splay complex, *sensu* Mjøs *et al.*, 1993; Miall, 1996).

Facies Association 9: Distal floodplain

Description

Facies Association 9 (FA 9) is characterized by red (colour 10R 3/4), massive mudstones (Fm) with abundant pedo-features such as rhizoliths, mottles, nodules, cutans, mesofauna bioturbation (earthworms, trace fossils and *Taenidium* isp.) and slickensides (Tables 1 and 2; Fig. 4I). FA 9 is also characterized by granular, subangular, blocky and wedge-shape peds as the main pedogenic structures. The geometry of FA 9 is tabular with horizontal and sharp bounding surfaces. Facies packages range in thickness from a few centimetres up to 10 m and may be up to 1000 m in lateral extent.

The most diagnostic macromorphological pedo-feature (both in outcrop and cores) is the presence of slickensides characterized by cross-cutting curved surfaces forming bowl-like structures as well as wedge-shape peds. Other key pedogenic features, are the gley colour mottles (colour 5G 7/1), gley rhizoliths (colour 5G 5-7/1) and Fe-Mn nodules. In thin section, the cross-striated b-fabric and the presence of thin clay and both Fe-Mn oxide coatings and infillings are the most diagnostic micro-scale pedo-features (Table 2, Fig. 4I). X-ray diffraction analyses indicate that illite is the main component within the clay fraction. FA 9 is thus characterized by palaeosol profiles with Ass(?)–Bss–C successions. The surface palaeosol horizons (Ass horizons) are, however, usually absent, and where present can only be recognized by the granular ped structures reflecting poorly developed horizonation.

The GR log through FA 9 is characterized by higher API values, compared to the facies associations described above, and shows an aggrading trend (Fig. 4I). The OBI and ABI logs are characterized by a massive and homogeneous aspect, lacking any clear surfaces except the presence of very high angle sine waves in two opposing preferential directions (Fig. 4I).

Interpretation

This facies association is interpreted as the deposits of a distal floodplain characterized by widespread palaeosol development. The abundance of vertic pedo-features (slickensides, wedge-shape peds and cross-striated b-fabric) suggests the presence of shrinking and swelling expansive clays, although this apparently contradicts the X-ray diffraction analyses that show abundant illite. However, the illitization of smectites in palaeo-Vertisols due to burial diagenesis is a common process (Driese *et al.*, 2000) and may explain this apparent contradiction. The cross-cutting curved surfaces, forming bowl-like structures, are interpreted as the microlow areas of gilgai microrelief. In this sense, the poorly developed horizonation most likely records the mixing of seasonal shrink–swell processes (Driese *et al.*, 2000; Retallack, 2001; Varela *et al.*, 2012). The presence of hydromorphic features (Fe-Mn nodules, gley mottles and rhizoliths) also indicates seasonal waterlogged drainage conditions (Retallack, 2001). These pedo-features are also consistent with Vertisol-like palaeosol (Soil Survey Staff, 1998). The serrated shape (aggrading trend) of the GR log through FA 9 is also typical of fluvial floodplain deposits (Emery & Myers, 1996; Cant, 2002). The very high angle sine waves observed in OBI and ABI could be related to slickenside surfaces.

Facies Association 10: Swamp

Description

Facies Association 10 (FA 10) is composed of dark grey to dark purple (colours N2.5/0 to 10B 3-4/1) thin-laminated mudstones (Fl) and organic matter. Sporadic, thin, massive micritic limestones and massive mudstone lamina also occur. The geometry of FA 10 is tabular with horizontal and sharp bounding surfaces. Facies packages range in thickness from several centimetres up to 2 m with up to 100 m of lateral extension (Tables 1 and 2; Fig. 4J). Locally, desiccation cracks occur towards the top of the FA 10 succession.

The GR log through FA 10 is characterized by a serrate profile (aggrading trend) with the highest API values in comparison with FA 9. The OBI and ABI logs both show a high contrast, high amplitude base and top, between which multiple, parallel surfaces dipping <5 degrees, are observed (Fig. 4J).

Interpretation

Facies Association 10 is interpreted as having been deposited from suspension in a swamp environment. The dark grey and dark purple colours indicate reducing and anoxic conditions, with organic matter commonly preserved. The presence of desiccation cracks, as well as the transition to FA 9 most likely records swamp desiccation during dry seasons. The high API values characteristic of the GR log are probably due to an increase in the uranium associated with the organic matter (Myers & Bristow, 1989; Rider & Kennedy, 2011). Multiple, parallel, flat-lying surfaces, seen in OBI and ABI logs represent thin laminations accumulated by fall-out from suspension in extremely low energy conditions.

STRATIGRAPHIC ARCHITECTURE OF THE MUDSTONE–SANDSTONE UNIT

The exceptional outcrops of the study area permit a full description of the architectural elements of the M-S unit, as well as characterization of both the vertical and lateral variability of the previously described facies associations. From this it can be seen that the main channel and point bar deposits pass laterally into floodplain and swamp deposits interbedded with the crevasse-splay complex deposits recorded in the PNV-1 section as shown in Fig. 5.

Amalgamated crevasse-splay deposits occur throughout but are clearly more frequent towards the eastern edge of the outcrop, although still interbedded with an abundance of floodplain and swamp deposits. Towards the western part of the outcrop, the corresponding main channel and point bar deposits occur (Fig. 5). Finally, towards the top of this outcrop, main channel and point bar deposits occur where the PNV-1 section is located and grade laterally into the crevasse-splay deposits to the east of the outcrop (Fig. 5).

CHANNEL-CREVASSE-SPLAY COMPLEX MODEL

Outcrop perspective

The 18 sedimentary logs, constructed following the same stratigraphic level (Fig. 6), provide a framework from which the dimensions, lateral variability, and heterogeneities of the M-S Unit can be established. Towards the south-east (CPMR1 to CPMR8), a facies transition is observed, from the main channel (CP 0), through point bar, proximal to distal crevasse-splay complex, and finally distal floodplain deposits (Fig. 6). In contrast, towards the north-west (CPML1 to CPML9), the facies transition observed is from main channel to point bar to scroll bar and, finally, proximal and medial crevasse-splay complex (Fig. 6).

Through the empirical determination of the lateral facies variations, the internal discontinuities and the scale (lateral and vertical measurements) of the geo-bodies, as well as the distance to the main channel (Fig. 6), a conceptual model has been developed, as illustrated in Fig. 7. The key elements are summarized as follows:

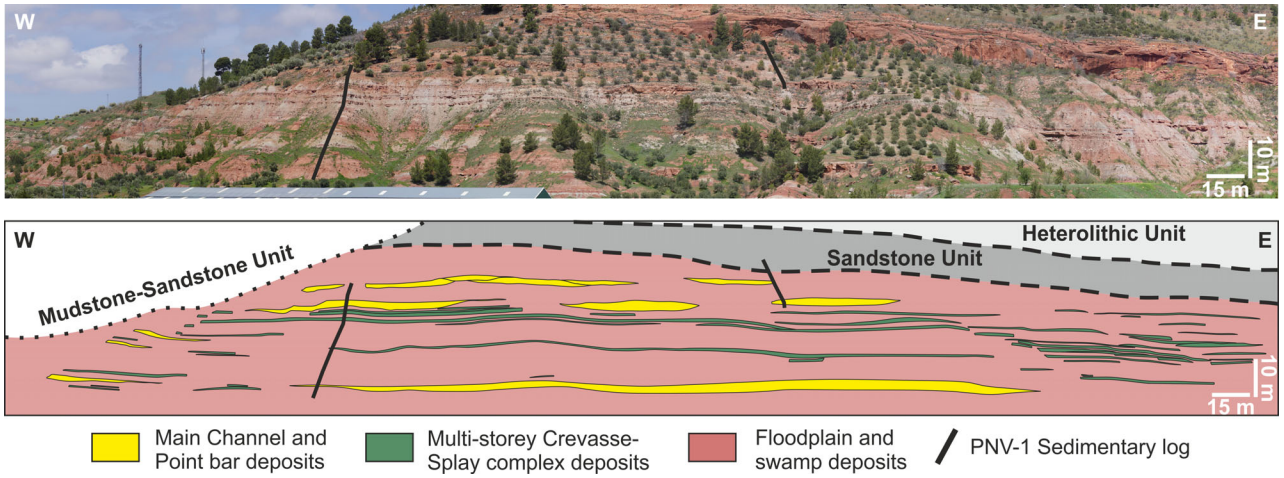

Fig. 5. West–East oriented panoramic view showing the key outcrop of the Mudstone–Sandstone Unit and interpretation of the main channels, multi-storey crevasse-splay complexes, distal floodplain and swamp deposits.

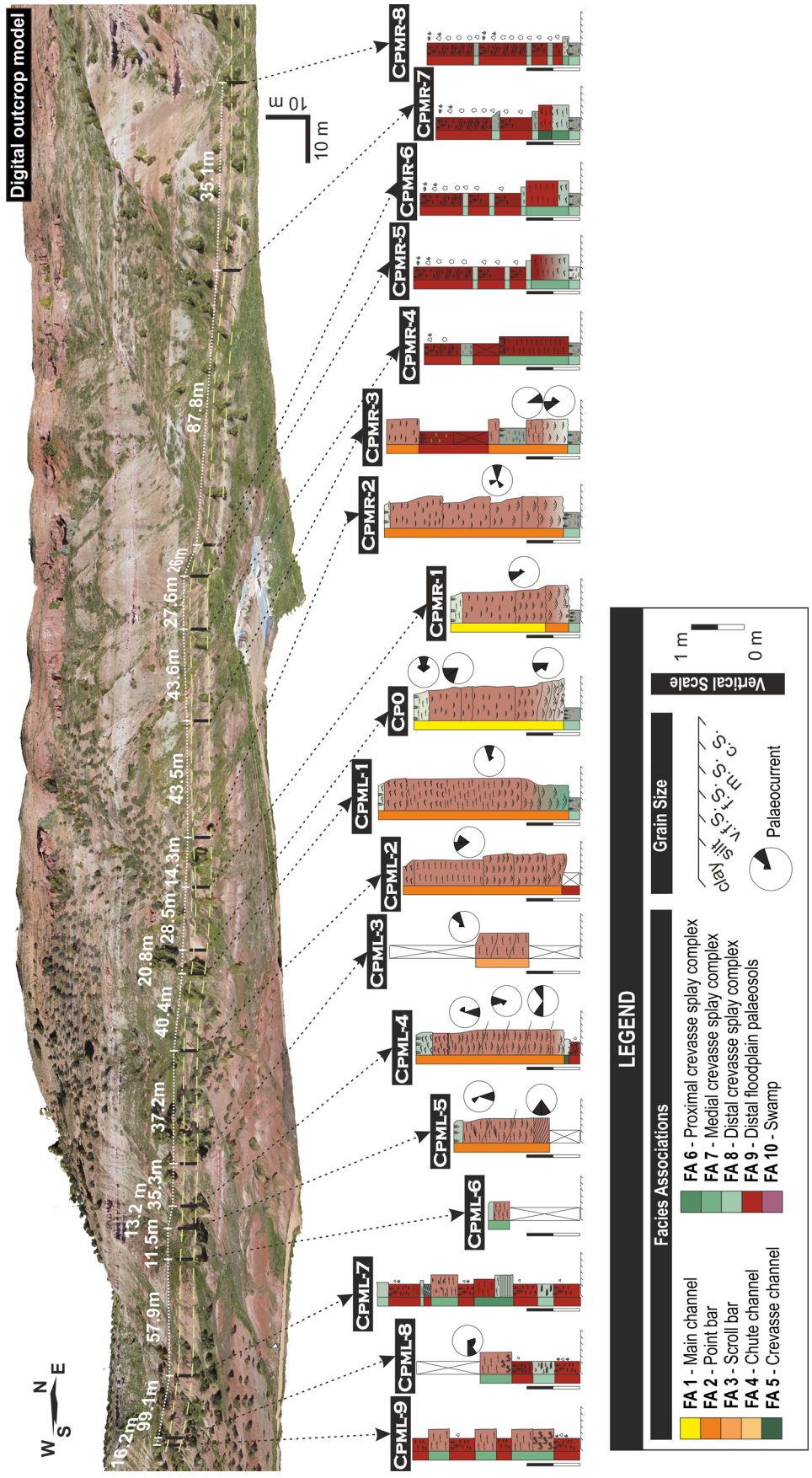

Fig. 6. Digital outcrop model (DOM) showing the location and measured distance between each of the sedimentary logs constructed in order to characterize lateral variability in facies sequences.

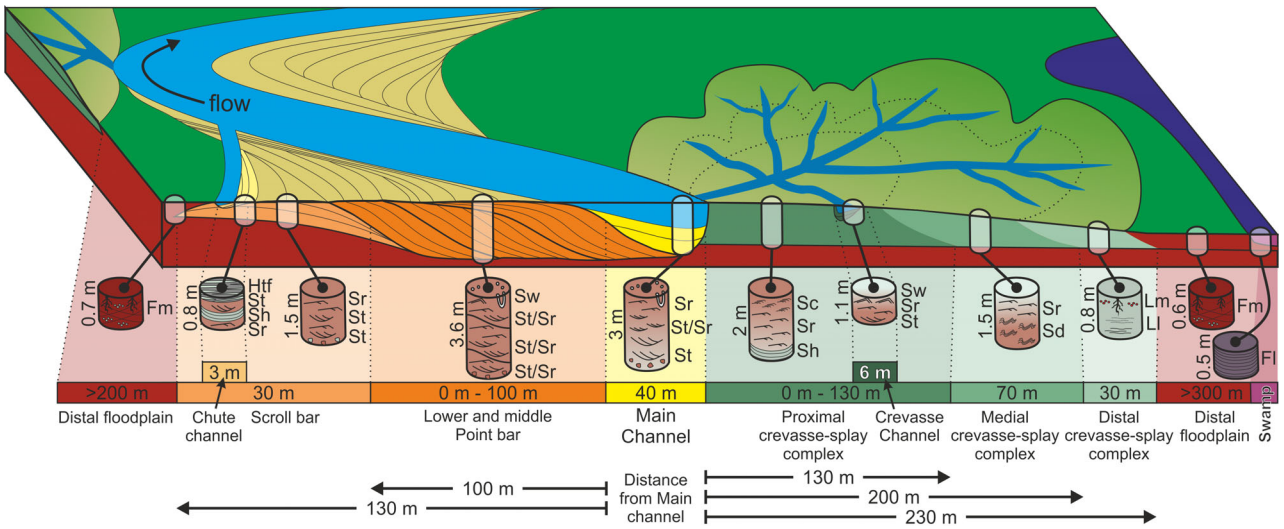

Fig. 7. Conceptual model of lateral variability for Facies Associations (FA 1 to FA 10) including sedimentary and pedogenic features, lateral extent or width of the associated depositional area and thickness of each facies association.

The main channel (FA 1) is 40 m wide and 3 m thick. On the accretional, inner margin of the thalweg, the main channel grades into lower and middle point bar deposits (FA 2).

The point bar is up to 3.6 m thick and 100 m wide, extending from the main channel. The deposits of the point bar pass into scroll bar deposits (FA 3). The scroll bar is up to 1.5 m thick, 30 m in width and located up to 130 m away from the main channel. Locally, chute channel deposits (FA 4) are incised into the scroll bar (Fig. 4D). These are up to 3.0 m in width and up to 0.8 m in thickness. The scroll bar grades laterally into distal floodplain deposits (FA 9).

On the erosive margin of the main channel, the crevasse-splay complex comprises a proximal crevasse-splay complex (FA 6) up to 130 m in width and up to 2 m thick. Crevasse channel (FA 5) deposits frequently cut into the proximal crevasse-splay complex (Figs 4E, 8A and 8B; Bristow *et al.*, 1999). Crevasse channels are up to 6.0 m wide and up to 1.1 m thick. The proximal crevasse-splay complex passes from the main channel into the medial crevasse-splay complex (FA 7), and is 70 m wide and 1.5 m thick. This is located 200 m away from the main channel and is also cut by crevasse channels. The distal crevasse-splay complex (FA 8) is located up to 230 m from the main channel. It is 30 m wide and 0.8 m thick. The distal crevasse-splay complex grades laterally into the distal floodplain (FA 9).

Distal floodplain deposits occur up to 300 m from the main channel. They vary between 100 m and 1000 m in width forming packages only 0.6 m thick. Locally, within the distal floodplain, swamp deposits (FA 10) occur which are up to 100 m wide and 0.5 m thick.

Sandstone geo-bodies interpreted as crevasse-splay deposits in the M-S Unit have a lobate form marked by a sharp base and convex-up top. The dimensions of these deposits range from tens to hundreds of metres in width, with a thickness of 0.5 to 2.0 m (Fig 8A and B). These lobular geo-bodies rarely occur as a single crevasse-splay lobe generated during a flood event. Rather they are formed during continuous flood events leading to overlapping lobe geo-bodies, giving rise to a crevasse-splay complex (Fig. 8C and D).

A detailed interpretation of the crevasse-splay complexes (Fig. 8A and B) shows the amalgamation and architecture of the crevasse channel, proximal, medial and distal crevasse-splay deposits (FA5 to FA8) (Fig. 8B). Internally, each crevasse-splay complex also displays a vertical, progradational, trend from distal crevasse (FA 8) to medial and proximal crevasse-splay (FA 7 and FA 6, respectively). Locally, however, distal crevasse-splay deposits are observed overlying proximal crevasse-splay deposits (Fig. 8B).

Measurements from DOM (Fig. 8B) show up to 2.1 m thickness for crevasse-splay lobes with

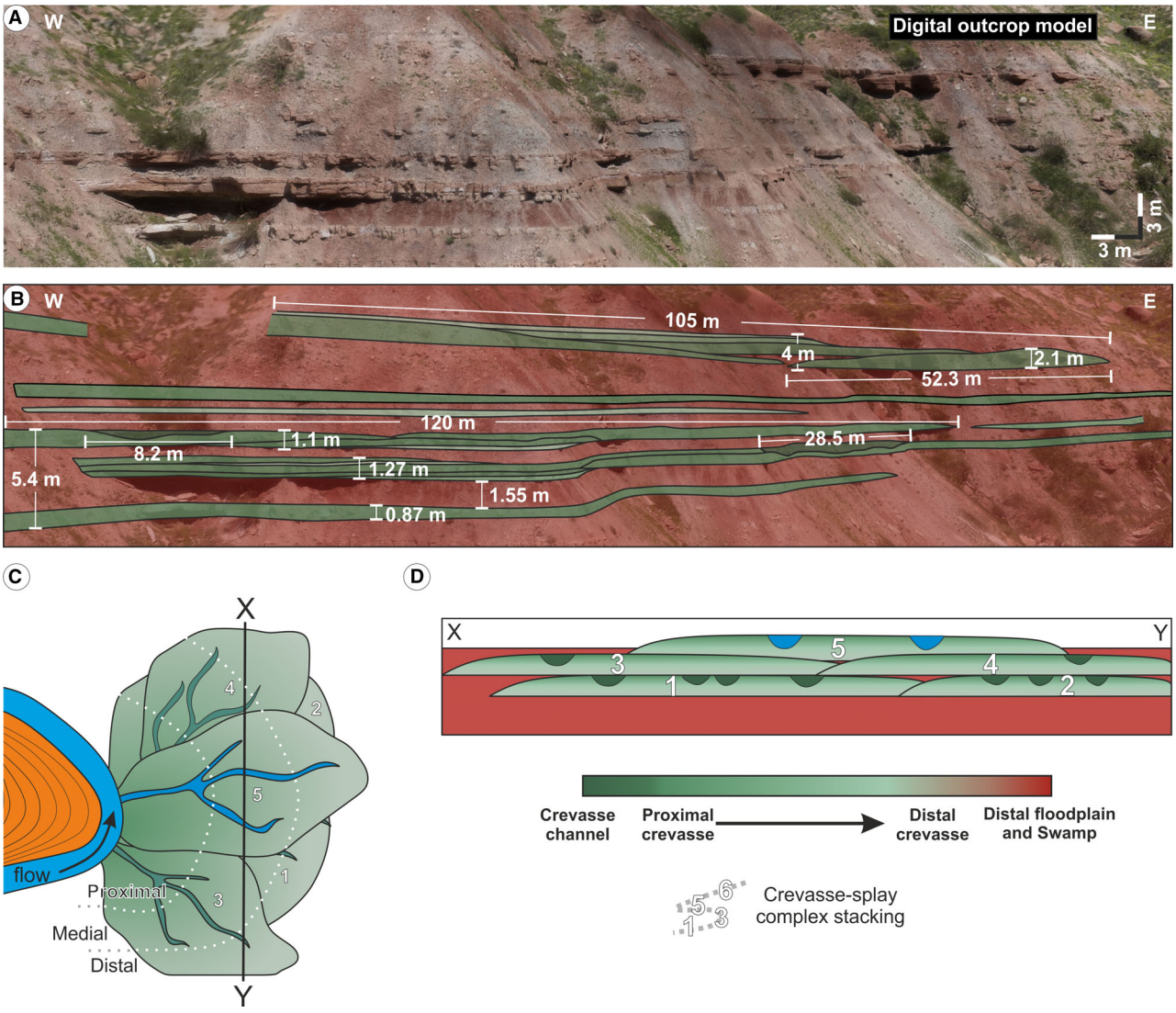

Fig. 8. (A) and (B) Close-up view of crevasse-splay complexes showing a detailed interpretation of internal bounding surfaces and both lateral and vertical variability of the facies associations. (C) Plan-view conceptual model of a crevasse-splay complex. (D) Cross-section conceptual model of crevasse-splay complexes. Numbers in (C) and (D) are related to the order of deposition.

proximal crevasse-splay deposits (FA 6) and a width of up to 52.3 m measured approximately perpendicular to the lobe propagation direction (Fig. 8B). As described above, these crevasse-splay lobes appear to be amalgamated, forming a crevasse-splay complex. In the DOM section shown in Fig. 8B, the crevasse-splay complexes range from 1.1 m to 4.0 m in thickness (Fig. 8B). The dimensions for the crevasse channel, interpreted in this section, are 1.1 m thick and 28.5 m wide, measured sub-perpendicular to flow direction (Fig. 8B).

Subsurface perspective

From the comparison between the largely complete outcrop sedimentary log (PNV-1; see Fig. 1 for locations) and the two wells (S2P4 and K2P1), located at distances of 405 m and 275 m, respectively (Fig. 9), it can be seen that the sequence of facies associations corresponds to the stacking of the various architectural elements.

From base to top, the lowest two thirds of the PNV-1 section comprises distal floodplain and swamp deposits (FA 9 and FA 10) interbedded

with crevasse-splay complex facies (FA 5 to FA 8). In this interval, the palaeocurrent measurements fall into two main groups; north-east-directed and south-east-directed for the crevasse-splay deposits. In contrast, in the uppermost third of the PNV-1 section; main channel and point bar (FA 1 and FA 2) deposits show a mean palaeocurrent direction towards the north (between N280E and N095E; Fig. 9).

In the cored section from Well K2P1, towards the base, point bar deposits (FA 2) are observed. These are overlain by distal floodplain and swamp (FA 9 and FA 10) deposits, interbedded with crevasse-splay complex (FA 5 to FA 8) facies (Figs 9 and 10A). In Well S2P4 the core comprises distal floodplain and swamp (FA 9 and FA 10) deposits interbedded with crevasse-splay complex (FA 5 to FA 8) facies (Figs 9 and 11A). This well did not penetrate either main channel and/or point bar (FA 1 and/or FA 2) facies.

The GR logs from both Wells S2P4 and K2P1, show a predominance of coarsening/cleaning-upward trends (funnel shapes) which reflect a progradation from distal floodplain to crevasse-splay deposits (FA 9 to FA 5) and/or from distal to proximal crevasse-splay deposits (FA 8 to FA 5; Fig. 9). To a lesser extent, fining-upward trends (bell shapes) also occur (Figs 9, 10B and 11B). These correspond to main channel deposits (FA 1), crevasse channel deposits (FA 5) with a shift from proximal (FA 6) to distal (FA 8) crevasse-splay deposits. In contrast, the aggrading trends (serrated GR profiles) represent distal floodplain and/or swamp deposits (FA 9 and/or FA 10; Figs 9, 10B and 11B).

In Well K2P1, a total of 60 dip tadpoles were picked within crevasse-splay deposits with a mean azimuth of N093E, measurements ranging from N013E to N353E with the most frequent values between N014E and N137E. In point bar deposits (FA 2) a total of 45 dip tadpoles were picked with a mean azimuth of N346E (Figs 9 and 10B). In this Well, a 5.2 m thick interval is shown in Fig. 10, as an example of such a crevasse-splay complex. High-resolution analysis of dip tadpoles, for the basal 3.6 m of this interval, shows three discrete palaeocurrent packages, with azimuths, from base to top, of N092E, N044E and N134E (Fig. 10B), respectively. This suggests the stacking of three component crevasse-splay lobes. These lobes, in addition to prograding across the floodplain during flood events, are arranged laterally by compensation of accommodation space. Above this basal 3.6 m a bell-shaped GR profile is observed corresponding to medial and distal crevasse-splay deposits, respectively (Fig. 10B). In this interval, two dip tadpole packages are distinguished, with palaeocurrent directions to N015E and N094E, respectively. This superposition of distal over proximal facies, and with different palaeocurrent directions, strongly supports the interpretation of an amalgamated crevasse-splay complex.

In Well S2P4, a total of 236 dip tadpoles have been picked within crevasse-splay deposits with a mean azimuth of N081E, although there is a significant dispersion in palaeocurrent directions (360°). Dip tadpole analysis shows that: (i) in the lowest third of the section mean palaeocurrent values range between N065E and N247E; and (ii) the uppermost two-thirds of the section shows mean values ranging from N058E to N137E (Figs 9 and 11B).

From the foregoing descriptions of outcrop and well sections, the key features in core, GR log and palaeocurrent, for each of the main facies associations, are summarized as follows and in Figs 4, 12 and 13:

Main channel (FA 1) packages are distinguished by the stacking of several fining-upward (bell-shape) profiles in the GR log characterized by values ranging from 65 to 188 API (Fig. 12). The higher API values between each package represent mudstone rip-up clast conglomerates (Gp), occurring as basal lags. This pattern reflects the stacking of lithofacies Gp–St–Sr (Selley, 2004; Viseras *et al.*, 2018). Dip tadpole plots highlight several surfaces with dip angles of <15° and azimuths perpendicular to the dip tadpoles associated with the accretion surfaces. These dips correspond to the channel base erosional surfaces. Between these erosional surfaces, a set of dips with both random azimuth and dip angles between 5° and 25° are recorded (Fig. 13). These correspond to trough cross-bed foresets (Donselaar & Schmidt, 2005; Viseras *et al.*, 2018; Yeste *et al.*, 2018).

The point bar (FA 2) is characterized by a coarsening-upward or cleaning-upward (funnel shape) GR profile at the base, and a fining-upward (bell shape) towards the top of each facies package (Fig. 13), API values ranging from 35 API to 182 API (Fig. 12). The lowermost bell-shaped GR packages also show higher API values reflecting the presence of mudstone rip-up clasts (Selley, 2004; Viseras *et al.*, 2018). In core, point bar deposits are recognized by sets of lithofacies St–Sr separated by inclined surfaces corresponding to the lateral accretion surfaces.

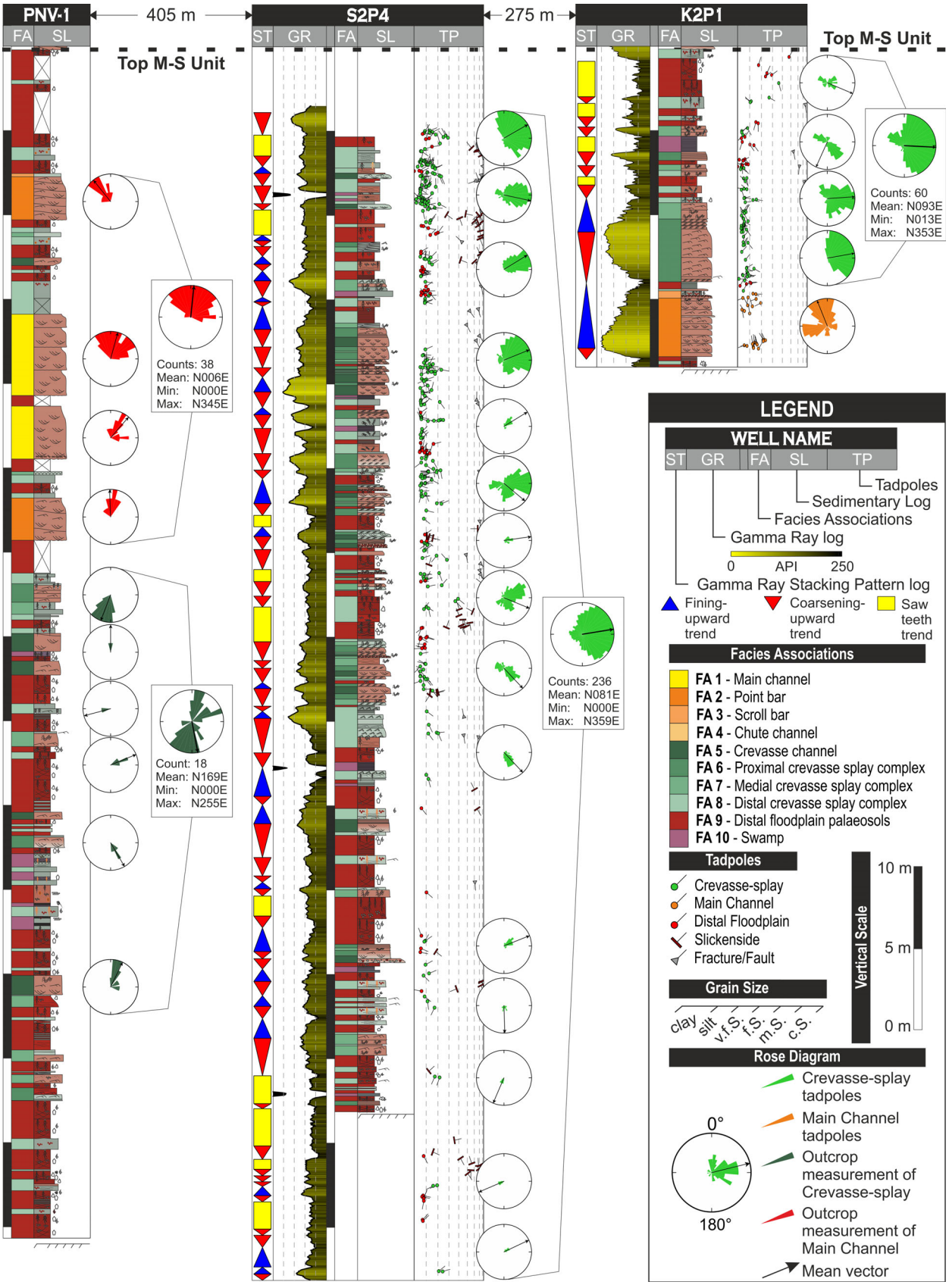

Fig. 9. Vertical variability of facies associations from outcrop and subsurface data. Section PNV-1 data is outcrop-derived including sedimentological log, facies associations and palaeocurrent data. S2P4 and K2P1 are wells (see Fig. 1 for location) which include Gamma Ray (GR) log, GR stacking patterns, core description, facies associations and palaeocurrent measurements from borehole images. The rose diagrams inside the rectangle show the measurements for the indicated interval.

Two dip tadpole groups are associated with this facies association: (a) shallow-to-steep-to-shallow dip angles towards the top (Fig. 13); and (b) azimuths displaying a slightly variable rotation (clockwise or anticlockwise) towards the top. These tadpoles correspond to lateral accretion surfaces (Donselaar & Schmidt, 2005; Brekke *et al.*, 2017; Viseras *et al.*, 2018). Tadpole sets with random azimuth and dip angles between 5° and 25°, occurring between the planar features of (a) are interpreted to represent trough cross-bed foresets (Donselaar & Schmidt, 2005; Viseras *et al.*, 2018; Yeste *et al.*, 2018).

Proximal crevasse-splay deposits (FA 6) are characterized by a coarsening-upward or cleaning-upward (funnel shape) GR response truncated by a sharp top (Fig. 13), API values ranging from 57 API to 197 API (Fig. 12). In core, this association is characterized by the lithofacies succession Sh–Sr–Sc indicating flow deceleration and significant deposition during splay events (Burns *et al.*, 2017). Locally, the funnel-shaped GR profile develops into a bell-shape (fining-upward trend) towards the top of the facies package reflecting truncation by crevasse channel deposits (FA 5). This bell-shaped GR package corresponds, in core, with the lithofacies succession St–Sr–Sw implying a gradual flow deceleration and overbanking of the crevasse channels (Bristow *et al.*, 1999; Burns *et al.*, 2017). FA 6 is characterized by tadpoles with unidirectional azimuths and dip angles of <10° (Figs 11C, 11E and 13). In contrast, FA 5 is characterized by sets of tadpoles with randomly distributed azimuth and dip angles between 5° and 25° (Figs 11D, 11E and 13). Towards the top, this association typically shows a tadpole set with unidirectional azimuth and dip angles <10°.

Medial crevasse-splay deposits (FA 7), are characterized in core by the presence of syn-sedimentary deformation indicating rapid sediment accumulation onto a water-saturated substrate (Bristow *et al.*, 1999; Rossetti & Santos, 2003; Owen & Santos, 2014; Burns *et al.*, 2017). These deposits also comprise lithofacies Sr and, occasionally, Sd. The associated GR profile is characterized by a coarsening-upward or cleaning-upward trend (funnel shape), API values ranging from 99 API to 200 API (Fig. 12). Tadpoles in FA 7 are characterized by randomly distributed dip angles and azimuths when syn-sedimentary deformation structures (Sd) are present (Figs 11F and 13). In the interval where FA 7 is characterized by Lithofacies Sr, the tadpole pattern shows a unidirectional azimuth and dip angles of <10°.

Distal crevasse-splay deposits (FA 8) are also characterized by funnel-shaped (coarsening-upward or cleaning-upward trend) GR packages, albeit notably thinner than those associated with medial or proximal crevasse-splay deposits. The API values range from 99 API to 242 API (Fig. 12). In core, FA 8 is characterized by lithofacies Lm and Ll suggesting poorly-developed palaeosols (Retallack & Dilcher, 2012). The dip tadpoles through this association clearly highlight the bounding surfaces (bottom and top) of each package. Locally, where Lithofacies Ll is present, very low dip angle tadpoles (<10°) with unidirectional azimuths are recognized (Fig. 13).

Distal floodplain deposits (FA 9) are characterized by a typically serrated GR response (aggrading trend) with high API values (ranging from 105 API to 244 API; Figs 12 and 13). In core, FA 9 is characterized by red, massive mudstones with abundant vertic pedo-features (lithofacies Fm), suggesting Vertisol-like palaeosols (Soil Survey Staff, 1998). Two dip tadpole types are identified in FA 8: (i) tadpoles with very low dip angles (<7°) and a unidirectional azimuth; and (ii) tadpoles with very high dip angles (30° to 75°) and a bi-directional azimuth; the latter are associated with slickensides structures (Figs 11B and 13).

Swamp deposits (FA 10) show the highest GR values in the M-S Unit (ranging from 110 API to 366 API; Fig. 12) and a characteristically serrated GR profile (aggrading trend). In core, FA 10 is characterized by dark grey to dark purple-coloured, thinly-laminated mudstone (lithofacies Fl). FA 10 is also characterized by tadpoles with very low dip angles (<10°) and unidirectional azimuths (Figs 11B and 13).

DISCUSSION

The detailed study of lateral facies variability using both outcrop and subsurface data (core,

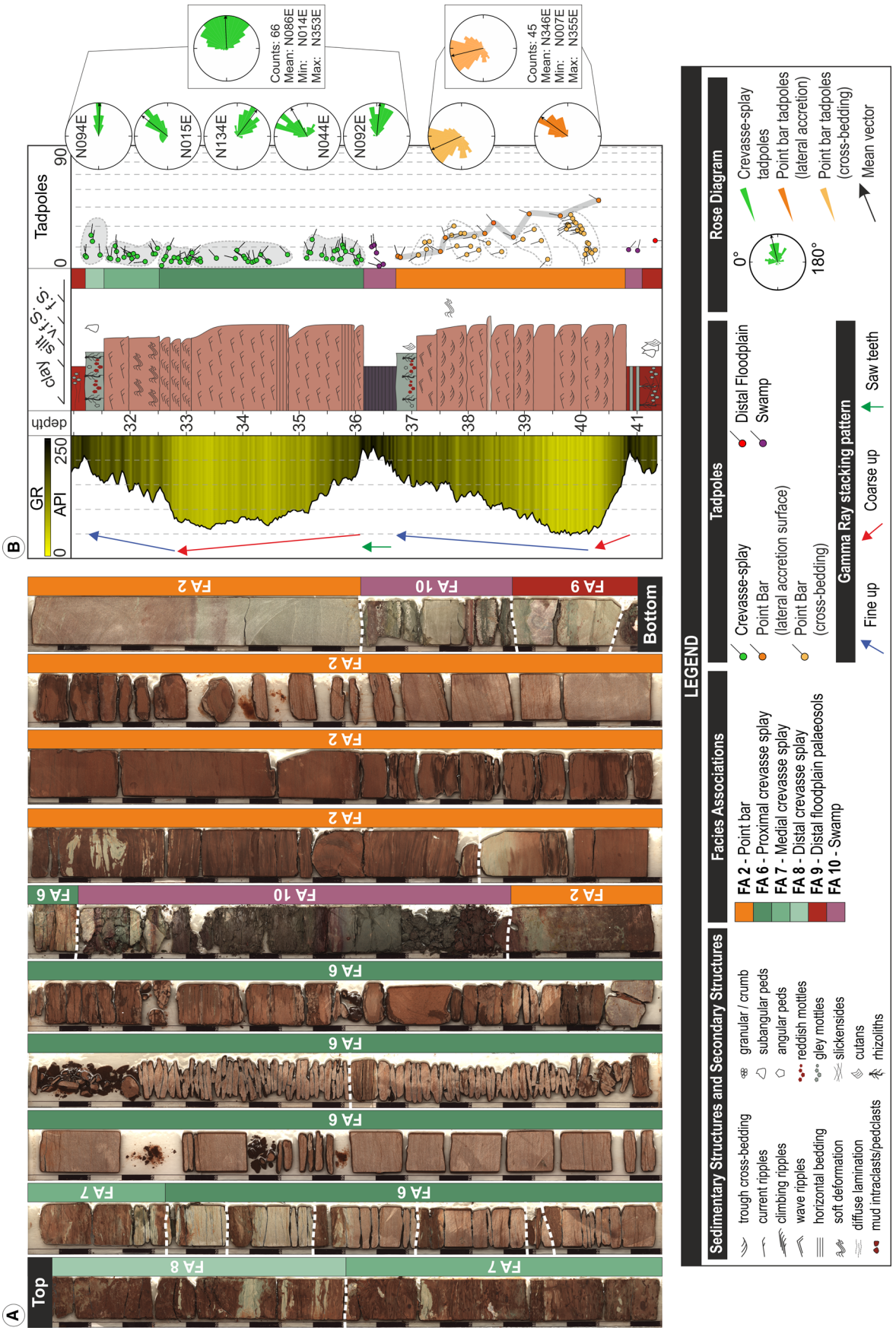

Fig. 10. (A) Core view showing a 10 m thick interval (from 31 m to 41 m depth) of Well K2P1. (B) K2P1 well composite (31 to 41 m depth interval) displaying the Gamma Ray (GR) log, the core description, facies associations interpretation and dip tadpole analysis. Red and blue arrows indicate a coarsening-upward, cleaning-upward or fining-upward GR profile, respectively.

GR log and image log data) of the study area has enabled the definition of ten facies associations. Furthermore, with DOM data, it has also been possible to make precise measurements of both thickness and width for each of these facies associations and thereby define their geometric characteristics. In addition, the full integration of subsurface datasets and their validation with surface equivalents has enabled the development of more realistic conceptual models that include both descriptive and quantitative data related to the distribution of heterogeneities within the M-S Unit (Figs 7 and 13).

The predictive conceptual model presented in this study helps to reduce uncertainty surrounding the location and dimensions of the key channel element (main reservoir) on a low gradient floodplain. The proposed model only uses data essentially identical to that which would be acquired during exploration and production drilling of wells located across a floodplain. This is critical for the establishment of a more robust basis for predicting the location of primary and secondary reservoirs, in low net-to-gross fluvial settings, with greater precision and significantly reduced risk.

The method is applied to an example that has been shown to be an excellent outcrop analogue for fluvial reservoirs. More specifically, the M-S Unit is an excellent outcrop analogue for the lower TAGI (Trias Argilo-Gréseux Inférieur) in the Berkine Basin, Algeria (Rossi *et al.*, 2002; Viseras *et al.*, 2011; Henares *et al.*, 2014). Recent studies (e.g. Burns *et al.*, 2017; Gulliford *et al.*, 2017; Ielpi *et al.*, 2018), also suggest how the predictive model presented here could be used as an analogue for low net-to-gross fluvial reservoirs with different ages but with similar geobody dimensions. Varela *et al.* (2019) have also established a comparative relationship between palaeosol development and the fluvial architecture of sedimentary successions from both the Cretaceous of Patagonia, Argentina and Triassic Red Beds of Iberian Plateau (TIBEM). The authors have recognized an increase in maturity within the palaeosol catena moving away from the main channel bodies. The most mature palaeosol was, in each case, located at similar distance (200 to 300 m) from the main channels. Gil-Ortiz *et al.* (2019) have also identified a meandering fluvial-dominated system in the Lower Cretaceous pre-salt units of the distal offshore South Gabon sub-basin. These authors suggest similar dimensions and architectural elements (meandering channels and crevasse-splay lobes) from image log data. The quantitative conceptual model presented for the M-S Unit could equally be applied to this Cretaceous formation and potentially many other low net-to-gross fluvial successions worldwide.

Distribution of heterogeneities and evolution of crevasse-splay lobes

Recent studies in outcrop of crevasse-splay deposits have shown similar facies distributions and facies belt dimensions for the same architectural elements described for the M-S Unit. Burns *et al.* (2017), for example, have described facies distributions from the Cretaceous Castlegate Sandstone and Neslen Formations of Utah. Kraus & Aslan (1999) established the development of palaeosol catenas related to topographic relief and to distance from the main channel. Moscariello (2009) highlights the importance of palaeosol identification in low net-to-gross systems because palaeosol distribution is closely linked to channel sand distribution and reservoir architecture. Varela *et al.* (2012) have also carried out a quantitative study in the Cretaceous Mata Amarilla Formation, of Argentina, focussed on the spatio-temporal distribution of different palaeosols relative to the distance to the main channel. These authors also recognized an increase in maturity within the palaeosols catena with increasing distance from the main channel bodies, so that the most mature palaeosols are located in the distal floodplain at *ca* 200 m from the main channel. The current study also observed a palaeosol catena developed from distal crevasse-splay deposits (FA 8; Entisol-like) to distal floodplain deposits (FA 9; Vertisol-like). The measurements made in outcrop prove that the most mature palaeosols of this catena are located at >300 m from the main channel deposits (Fig. 7).

In the most common case, the stacking of distal to medial to proximal crevasse-splay deposits is explained by the progradation of the crevasse-splay facies belts in successive flood events (*sensu* Mjøs *et al.*, 1993; Miall, 1996; Bristow *et al.*, 1999). However, the occurrence of distal crevasse-splay deposits overlying a proximal crevasse-splay must be explained by the stacking of successive crevasse-splay lobes through lateral compensation of accommodation space (Li *et al.*, 2014; Li & Bristow, 2015; Fig. 8C). Because the stacking of successive crevasse-splay lobes is conditioned by lateral compensation, the propagation direction of lobes ranges

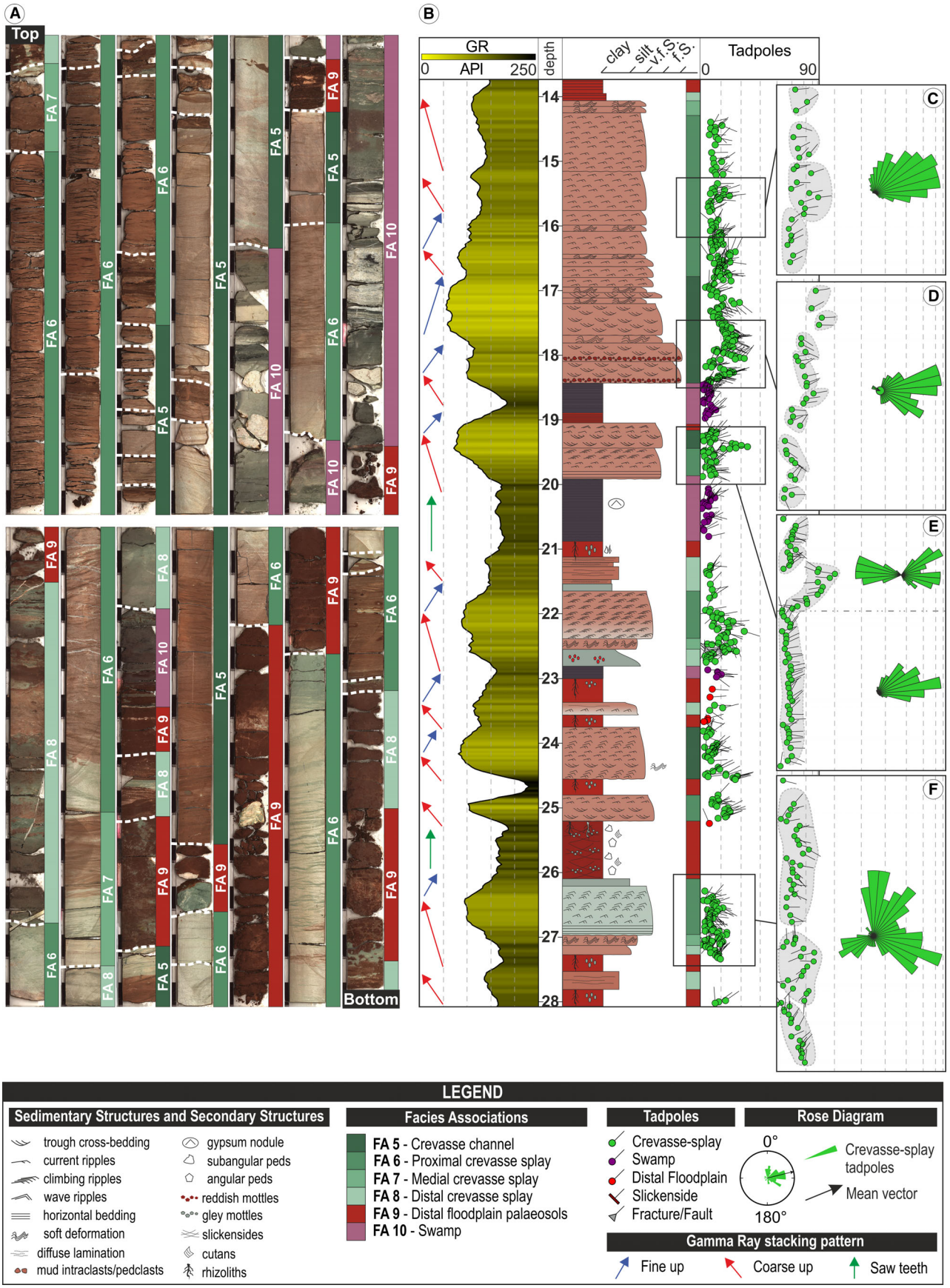

Fig. 11. (A) Core view showing a 14 m thick interval (from 14 m to 28 m depth) of Well S2P4. (B) S2P4 well composite (14 to 28 m depth interval) displaying the Gamma Ray (GR) log, the core description, facies associations interpretation and dip tadpole analysis. Red and blue arrows indicate a coarsening-upward, cleaning-upward or fining-upward GR profile, respectively. (C) to (F) Selected close-up view of dip tadpole log highlighting the grouping of tadpole patterns accompanied by a rose diagram for each interval.

from 15° to 130° relative to the main channel axis into the same crevasse-splay complex (Fig. 8C and D). This lateral and vertical amalgamation of lobes explains the significant areal extent of crevasse-splay complexes typical of the M-S unit (Mjøs *et al.*, 1993; Van Toorenenburg *et al.*, 2016; Burns *et al.*, 2017).

In addition, these crevasse-splay complexes may also stack to form amalgamated crevasse-splay complexes. In some sections, between two crevasse-splay complexes, distal floodplain and/or swamp deposits are observed (Fig. 8B). In other sections, a lateral overlap between two crevasse-splay complexes can also be observed (Fig. 8B), suggesting that these complexes may well be connected three-dimensionally when amalgamated.

The excellent preservation of these crevasse-splay deposits, even in proximal facies, is due to the tendency of main channels to suffer sudden avulsions, rather than processes of gradual abandonment, thereby preventing cannibalization, linked to erosion by channel migration (Burns *et al.*, 2017). Preservation is also more likely, considering that the system was located on a very low gradient alluvial coastal plain, in a context of sea-level rise which triggers frequent avulsion processes (Fernández & Dabrio, 1985; Henares *et al.*, 2014, 2016a,b; Viseras *et al.*, 2018).

Implications for subsurface prediction

The high-resolution analysis of GR log trends, corroborated by both outcrop and core data, strongly suggests that the predominant funnel-shaped GR response reflects proximal, medial and distal crevasse-splay deposits (Fig. 11B). This funnel-shape reflects the progradation of the overbank facies in successive flood events (*sensu* Mjøs *et al.*, 1993; Miall, 1996; Emery & Myers, 1996; Cant, 2002). An overlying fining-upward trend, with a distinctive bell-shaped GR response, marked by higher API values, and related to medial and/or distal crevasse-splay deposits, is interpreted to record amalgamation of crevasse-splay complexes (Figs 10B and 11B). The crevasse channel deposits show a bell-shaped GR trend associated with a characteristic vertical lithofacies succession (St–Sr–Sw).

A high-resolution analysis of dip tadpoles, grouping those with a sedimentological significance, corroborated by both outcrop and core data, is also useful in reducing the uncertainty in sandstone depositional trends (Donselaar & Schmidt, 2005).

Brekke *et al.* (2017) also recognize the shallow-to-steep-to-shallow dip pattern in point bar deposits in the McMurray Formation of Alberta. This pattern of change in dip angles reflects epsilon cross-bedding (Allen, 1983) and is characteristic of lateral accretion surfaces in point bars. Donselaar & Schmidt (2005) interpreted the azimuth rotation (clockwise or anticlockwise) as the expression of the gradual downstream migration of the meander bend. The azimuth rotation in this case is poorly developed. This can be explained if point bar migration occurred mainly by expansion, where the bend apex migrates transversely

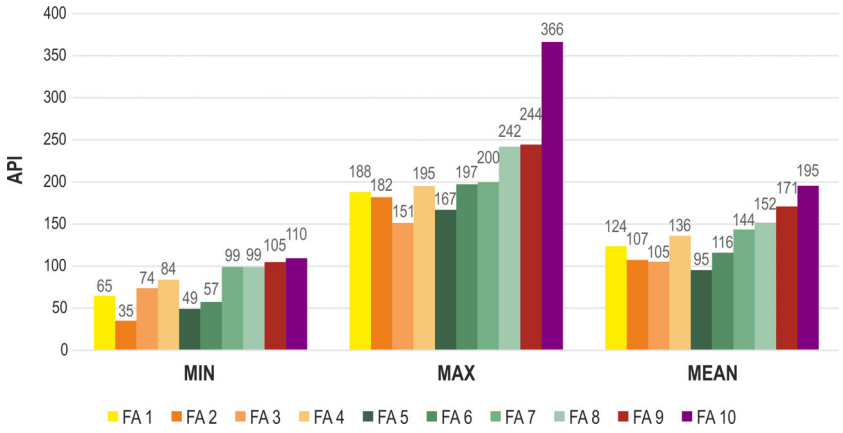

Fig. 12. Statistics summarizing the minimum, maximum and mean API values for each Facies Association.

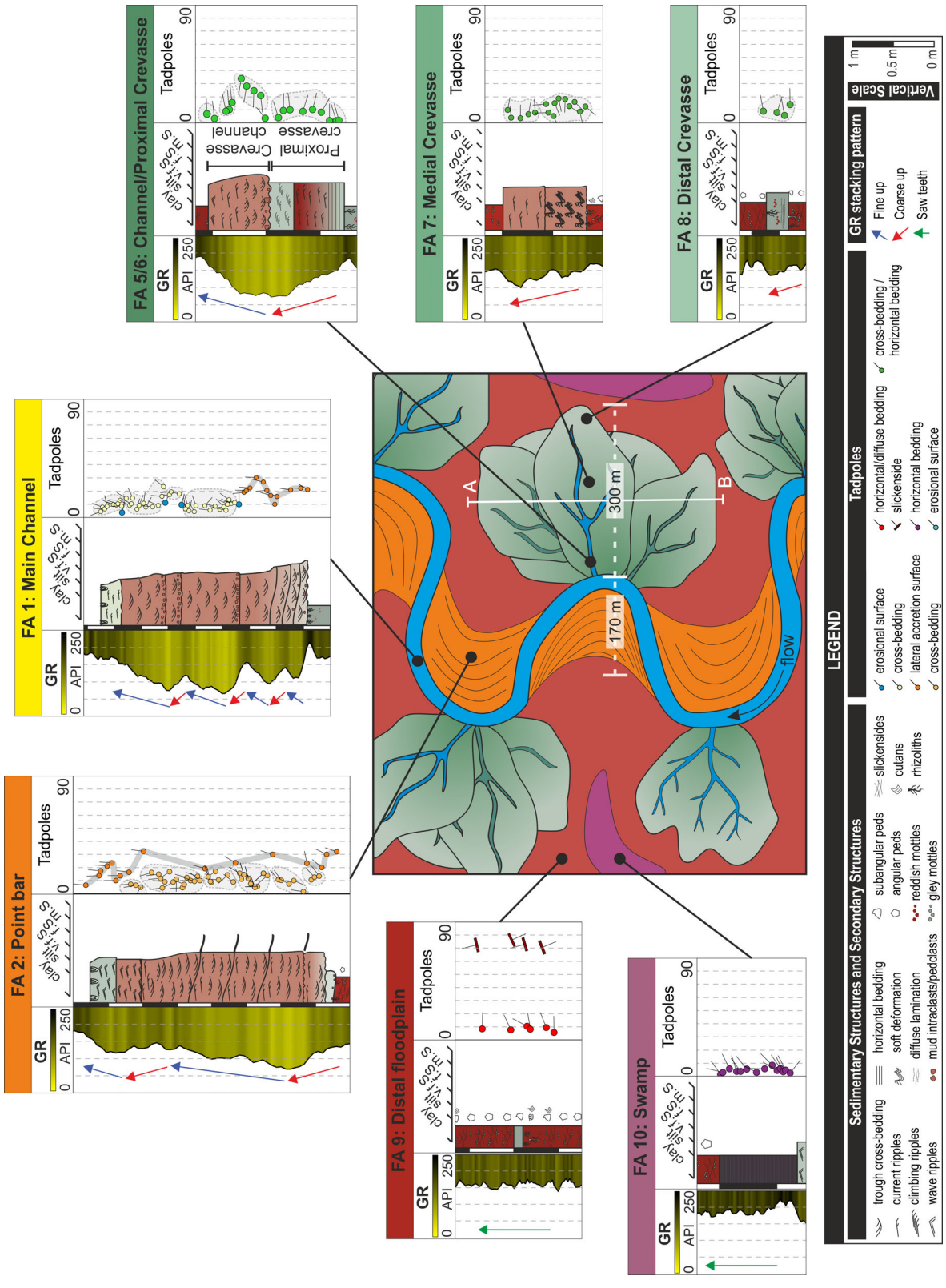

Fig. 13. Schematic plan-view of a conceptual model for the Mudstone–Sandstone Unit. This shows the key sedimentological, Gamma Ray log features and dip tadpole patterns for each facies association.

away from the channel-belt axis (Ghinassi *et al.*, 2014; Ielpi & Ghinassi, 2014). Tadpole sets with random azimuth and dip angles, between 5° and 25°, represent the foresets of trough cross-bedding (Donselaar & Schmidt, 2005; Viseras *et al.*, 2018; Yeste *et al.*, 2018).

Donselaar & Schmidt (2005) have also identified tadpole patterns with unidirectional azimuths and very low dip angles for crevasse-splay deposits. Keeton *et al.* (2015) highlighted the difficulty in picking tadpoles in crevasse-splay deposits reflecting the convoluted and ripple-laminated nature of the deposits, but recognized low angle dips and a high dispersion in dip azimuths. The high-resolution analysis of tadpoles in this study reveals patterns associated with the different segments of the crevasse-splay lobes (Fig. 13): (i) tadpoles with randomly distributed azimuth and dip angles between 5° and 25° due to trough cross-bedding in FA 5; (ii) tadpoles with unidirectional azimuths and low dip angles associated with horizontal and ripple-laminated sandstones in FA 6; (iii) randomly distributed dip angles and azimuths and unidirectional azimuths associated with low dip angles corresponding respectively to syn-sedimentary deformation structures and ripple-laminated sandstones, associated with FA7; and (iv) unidirectional azimuths and low dip angles between mud rock laminae in FA 8.

Implications for reservoir connectivity and modelling

The identification of amalgamated crevasse-splay complexes is of considerable importance because they can be considered potential hydrocarbon reservoirs (Van Toorenenburg *et al.*, 2016). Crevasse-splay deposits connect to the main channel body, which typically constitutes the best reservoir (Fielding & Crane, 1987; Pranter *et al.*, 2008). Proximal crevasse-splay and crevasse channel deposits comprise similar lithofacies, in addition to being directly connected to the main channel. Amalgamated crevasse-splay complexes can also be used to estimate the dimensions of the main channels in intervals where the channel body itself is not directly penetrated by a well. The thickness of the main channel will be similar to that of the amalgamated crevasse-splay complexes (Van Toorenenburg *et al.*, 2016). Thus, a detailed study of the proposed facies associations in core, and a high-resolution study of both GR log response and dip tadpole patterns would lead to a correct identification of depositional sub-environments, sediment body geometries, dimensions, orientations and thus a better estimate of net reservoir volume.

Recent studies related to the petrophysical and diagenetic characteristics of the M-S Unit (Henares *et al.*, 2014, 2016a,b) have established a strong relationship between Open Porosity (OP), permeability and early diagenetic processes. The latter are strongly related to depositional environments and thus the distribution of facies associations.

Although there is no systematic petrophysical and diagenetic study for crevasse-splay deposits (FA 5 to FA 8), it is reasonable to assume the same relationships between OP, permeability and early diagenetic processes. Henares *et al.* (2014) recognized 4.6% of gypsum cement associated with the crevasse-splay deposits in the M-S Unit. This cement occurs as poikilotopic crystals occluding primary porosity. These authors also report values of 15.6% of OP and 2mD of permeability for one sample of crevasse-splay deposits in the M-S Unit. These values reflect the pervasive influence of the gypsum in reducing permeability by occlusion of pore throats although subsequent patchy cement dissolution does act to generate the poorly connected secondary pores mentioned previously.

Henares *et al.* (2016a,b) also conclude that there is a good match between reservoir properties and facies distribution. This relationship is a direct consequence of the primary control exerted by depositional features, notably detrital clay abundance and distribution, on diagenetic evolution and thus on reservoir quality. As such, permeability will most probably be higher in those facies associations where grain coating clays are well-developed and significant primary porosity preserved. Conversely, those facies associations characterized by pervasive gypsum cement will show the poorest reservoir quality. This suggests that even the medial crevasse-splay facies (FA 7) could have favourable petrophysical characteristics, and thus be considered a potential hydrocarbon reservoir.

Through the combined integration of both outcrop and subsurface datasets, this study offers a new quantitative conceptual model for low gradient, meandering, fluvial systems, with key geometric and sediment body dimension data, which can be used in the elaboration of more robust numerical models. This is especially valuable for the crevasse-splay/floodplain elements which, otherwise, are not so well-understood and may often act as a secondary

reservoir. Such data can be used directly as input in reservoir modelling of similar subsurface systems. Quantitative conceptual models are a valuable tool in geostatistical modelling, especially when it comes to planning modelling strategies as well as producing training images. The detailed study of palaeosols and overbank deposits, and their integration into geostatistical modelling, also provides information on the position of the channel (main reservoir) in low net-to-gross reservoirs (Yeste *et al.*, 2019). Based on the OBO (Outcrop/Behind Outcrop) methodology this study suggests well-calibrated criteria for recognizing the key facies elements, from purely subsurface wireline log and core data; so that if key facies can be correctly identified in the subsurface, the outcrop geometry data can subsequently be applied as input for modelling.

Limitations of the predictive conceptual model

Although the potential applicability of the presented conceptual model to similar systems of different age is self-evident (Burns *et al.*, 2017; Gulliford *et al.*, 2017; Varela *et al.*, 2019,), it is nonetheless prudent to indicate that it should not be considered as a general predictive model. In this respect, there are a number of key limitations associated with the conceptual model, related to three main factors: (i) scale of the fluvial system; (ii) humidity and palaeoclimatic conditions; and (iii) the sequence stratigraphic framework.

The first factor is related to the scale of the fluvial system; especially the main channel from which the overbank deposits are derived. Thus, in fluvial systems dominated by a main channel with larger dimensions (depth and width) than those presented in this example, overbank deposits may be more extensively developed. However, the dimensional ratios of the different facies zones and their relationship with the distance to the main channel should still result in patterns similar to those established in the conceptual model.

The second limiting factor is related to the humidity and palaeoclimatic conditions of the floodplain. Palaeosol analysis suggests a seasonal climate reflected in the development of Vertisol-like profiles in distal floodplain deposits. This was most likely promoted by seasonal rainfall and/or variations in fluvial discharge (Driese *et al.*, 2000; Retallack, 2001; Varela *et al.*, 2012). The presence of swamp deposits with preserved organic matter, and both the gley mottles and rhizoliths of the Vertisol-like palaeosols evidence seasonal ponding in the studied M-S Unit. Consequently, the overbank flow is slowed by the presence of a still-water body (Bristow *et al.*, 1999). These floodplain conditions would tend to favour a reduced areal extent and lobe-shape geometry of the crevasse-splay deposits compared to those accumulating on a dry floodplain. In addition, a dry floodplain would be characterized by a more gradual transition between facies associations and also a reduced thickness for the crevasse-splay lobes, in comparison with the presented conceptual model.

Finally, it is important to consider the position of the fluvial system in the basin and the sequence stratigraphic framework in order to apply the conceptual model. The M-S Unit in the study area was most likely located on a very low gradient plain in the distal part of drainage system (Dabrio *et al.*, 2005; Viseras *et al.*, 2011, 2018; Henares *et al.*, 2014, 2016a,b). This is evidenced by the presence of wave reworking and trace fossils towards the top of channel and point bar deposits. The development of Entisol-like palaeosols in the crevasse-splay deposits may also indicate high sedimentation rates and avulsion, which would inhibit the development and maturity of soils in the studied M-S Unit. As such, it seems reasonable to assume that the conceptual model presented here could successfully be applied to high sinuosity fluvial systems located in the distal part of drainage system within a framework of rising base level, which would tend to favour the development of a frequently flooded floodplain (Bristow *et al.*, 1999).

CONCLUSIONS

Ten facies associations (including core and wireline log characteristics; Figs 4, 7 and 13) characterize the four architectural elements/sub-environments recognized in the mudstone–sandstone unit of the TIBEM (Triassic Red Beds of Iberian Meseta): (i) channelized sandstone bodies consisting of three facies associations (main channel, chute channel and crevasse channel); (ii) asymmetrical sigmoidal-shaped sandstone bodies consisting of two facies associations (point bar and scroll bar); (iii) lobe-shaped to sheet-like sandstone bodies consisting of three facies associations (proximal crevasse-splay, medial crevasse-splay and distal crevasse-splay); and (iv) sheet-like mudstone bodies consisting of two facies associations (distal floodplain and swamp).

Wireline log characteristics, constrained by Outcrop/Behind Outcrop (OBO) methodologies,

allow to distinguish, in subsurface, the four elements that constitute the crevasse bodies (this paper and others here cited) along a channel-floodplain cross-section: crevasse channel and proximal, medial and distal crevasse-splays. The Gamma Ray (GR) log is characterized by a fining-upward trend and a sharp base for crevasse channel deposits, whereas proximal, medial and distal crevasse-splay deposits are characterized by a coarsening/cleaning-upward trend and a sharp top. The GR API values (maximum, minimum and mean) increase from proximal to distal deposits. Distal floodplain and swamp deposits, in contrast, are characterized by a serrate GR profile. Crevasse channels are also characterized by randomly distributed palaeocurrent azimuths and foreset dips whereas proximal crevasse-splay deposits are characterized by unidirectional azimuths and low dip angles. Medial crevasse-splay deposits are characterized by sets of either randomly oriented palaeocurrent azimuths and dips, or unidirectional azimuths and low dip angle tadpole patterns. For distal crevasse-splay deposits the bounding surfaces (bottom and top) are easily distinguished whilst unidirectional azimuths and very low dip angle tadpoles occur locally.

A new outcrop analogue dataset for meandering, low gradient fluvial systems, including key geometric and sediment body dimension data, is presented in this paper. This is especially valuable for the crevasse-splay/floodplain elements which, otherwise, are not so well-known and may often act as a secondary reservoir. A predictive model generated from outcrop and subsurface data allows to estimate, with some confidence, how far a well drilled through crevasse-splay/floodplain deposit might be from a main channel and thus potential primary reservoir, a prediction of significant value in exploration and appraisal. Such data can also be used directly as both hard and soft input in reservoir modelling of similar subsurface systems during the development of a discovery.

The use of OBO methodology allows to establish a well-constrained link between recently refined outcrop facies models of channel-overbank systems and channel-crevasse sandstone reservoirs in the subsurface.

ACKNOWLEDGEMENTS

Funding was provided by the research project CGL2017-89618-R (AEI/FEDER, UE), the RNM369 Research Group (PAI) and by the Repsol-University of Granada agreement. The research stay of A.N. Varela was funded by the Coimbra Group Young Latin American Professor Scholarship and Argentinean National Research Council (CONICET) External Research Scholarship. The authors are indebted to the Consejería de Agricultura of Castilla-La Mancha (JCCM), the city hall of Alcaraz and Luis Fernández (landowners) for the drilling licenses. The authors also thank REPSOL EXPLORACION, CEPSA E.P and Crimidesa for their support. We thank the constructive reviews of both an anonymous reviewer and Ana Alonso-Zarza as well as the Associate Editor, Charlie Bristow.

DATA AVAILABILITY STATEMENT

The data that support the findings of this study are available from the corresponding author upon reasonable request.

REFERENCES

Ajdukiewicz, J.M. and **Lander, R.H.** (2010) Sandstone reservoir quality prediction: the state of the art. *AAPG Bull.*, **94**, 1083–1091.

Allen, J.R.L. (1983) Studies in fluviatile sedimentation: bars, bar-complexes and sandstone sheets (low-sinuosity braided streams) in the brownstones (L. Devonian), Welsh Borders. *Sed. Geol.*, **33**, 237–293.

Arche, A. and **López-Gómez, J.** (2014) The Carnian Pluvial Event inWestern Europe: new data from Iberia and correlation with the Western Neotethys and Eastern North America–NW Africa regions. *Earth Sci. Rev.*, **128**, 196–231.

Blakey, R.C. and **Gubitosa, R.** (1984) Controls of sandstone body geometry and architecture in the Chinle formation (Upper Triassic), Colorado Plateau. *Sed. Geol.*, **38**, 51–86.

Brekke, H., **MacEachern, J.A.**, **Roenitz, T.** and **Dastgard, S.E.** (2017) The use of microresistivity image logs for facies interpretations: an example in point bar deposits of the McMurray Formation, Alberta, Canada. *AAPG Bull.*, **101**, 655–682.

Briant, I.D. (1983) Facies sequences associated with some braided river deposits of the Late Pleistocene age from southern Britain. *Int. Assoc. Sedimentol. Spec. Publ.*, **6**, 267–275.

Bridge, J.S. (2001) Characterization of fluvial hydrocarbon reservoirs and aquifers: problems and solutions. *AAS Revista*, **8**, 87–114.

Bridge, J.S. and **Tye, R.S.** (2000) Interpreting the dimensions of ancient fluvial channel bars, channels, and channel belts from wireline-logs and cores. *AAPG Bull.*, **84**, 1205–1228.

Brierley, G.J. (1991) Bar sedimentology of the Squamish River, British Columbia: definition and application of morphostratigraphic units. *J. Sed. Petrol.*, **61**, 211–225.

Bristow, C.S., **Skelly, R.L.** and **Ethridge, F.G.** (1999) Crevasse splays from the rapidly aggrading, sand bed,

braided Niobrara River, Nebraska: effect of base level rise. *Sedimentology*, **46**, 1029–1047.

Browne, G.H. and **Slatt, R.M.** (2002) Outcrop and behind-outcrop characterisation of a late Miocene slope fan system, Mt. Messenger Formation, New Zealand. *AAPG Bull.*, **86**, 841–862.

Burns, C.E., **Mountney, N.P.**, **Hodgson, D.M.** and **Colombera, L.** (2017) Anatomy and dimensions of fluvial crevasse-splay deposits: examples from the Cretaceous Castlegate sandstone and Neslen formation, Utah, USA. *Sed. Geol.*, **351**, 21–35.

Cant, D.J. (2002) Subsurface facies analysis. *Geol. Surv. Can. Alberta*, **1**, 27–44.

Dabrio, C., **Fernández, J.** and **Viseras, C.** (2005) Triassic fluvial sandstones (Central South Spain) – an excellent analogue for the TAGI Reservoir of Algeria, European Association of Geoscientists and Engineers. *67th EAGE Conference and Exhibition, Field Trip Guides*, 1. Van Houten (Holanda), 35 pp.

Donselaar, M.E. and **Schmidt, J.M.** (2005) Integration of outcrop and borehole image logs for high-resolution facies interpretation: example from a fluvial fan in the Ebro Basin, Spain. *Sedimentology*, **52**, 1021–1042.

Driese, S.G., **Mora, C.I.**, **Stiles, C.A.**, **Joeckel, R.M.** and **Nordt, L.C.** (2000) Mass-balance reconstruction of a modern Vertisol: implications for interpreting the geochemistry and burial alteration of paleo-Vertisols. *Geoderma*, **95**, 179–204.

Durkin, P.R., **Boyd, R.L.**, **Hubbard, S.M.**, **Schultz, A.W.** and **Blum, M.D.** (2017) Three-dimensional reconstruction of meander-belt evolution, Cretaceous McMurray Formation, Alberta Foreland Basin, Canada. *J. Sed. Res.*, **87**, 1075–1099.

Emery, D. and **Myers, K.J.** (1996) *Sequence Stratigraphy*. Blackwell, Oxford, UK, 297 p.

Fernández, J. and **Dabrio, C.** (1985) Fluvial architecture of the Buntsandstein-facies Redbeds in the Middle to Upper Triassic (Ldinian-Norian) of the Southeastern Edge of the Iberian Meseta (Southern Spain). In: *Aspects of Fluvial Sedimentation in the Lower Triassic Buntsandstein of Europe* (Ed. Mader, D.), Lecture Notes in Earth Sciences, 411–435.

Fielding, C.R. and **Crane, R.C.** (1987) An application of statistical modelling to the prediction of hydrocarbon recovery factors in fluvial reservoir sequences. In: *Recent Developments in Fluvial Sedimentology* (Eds Ethridge, F.G., Flore, R.M. and Harvey, M.D.), SEPM Special Publication, **39**, 321–327.

Franke, D., **Hornung, J.** and **Hinderer, M.** (2015) A combined study of radar facies, lithofacies an three-dimensional architecture of an alpine alluvial fan (Illgraben fan, Switzerland). *Sedimentology*, **62**, 57–86.

Ghinassi, M. (2011) Chute channels in the Holocene high-sinuosity river deposits of the Firenze plain, Tuscany, Italy. *Sedimentology*, **58**, 618–642.

Ghinassi, M., **Nemec, W.**, **Aldinucci, M.**, **Nehyba, S.**, **Özaksoy, V.** and **Fidolini, F.** (2014) Plan-form evolution of ancient meandering rivers reconstructed from longitudinal outcrop sections. *Sedimentology*, **61**, 952–977.

Gil-Ortiz, M., **Tur, N.**, **García, D.**, **Leandro, F.**, **Jiménez, A.**, **Ochoa, M.**, **Net, L.I.**, **Fernandez, O.**, **Manrique, C.**, **García, V.** and **Macarena, N.** (2019) Sedimentology of pre-salt clastic reservoirs in the South Gabon sub-basin with image log tools. *34th IAS Meeting of Sedimentology*, 10–13 Sep 2019, Rome, Italy.

Gouw, M.J.P. and **Berendsen, H.J.A.** (2007) Variability of channel belt dimensions and the consequences for alluvial architecture: observations from the Holocene Rhine-Meuse delta (The Netherlands) and Lower Mississippi Valley (USA). *J. Sed. Res.*, **77**, 124–138.

Gulliford, A.R., **Flint, S.S.** and **Hodgson, D.M.** (2017) Crevasse splay processes and deposits in an ancient distributive fluvial system: the lower Beaufort Group, South Africa. *Sed. Geol.*, **358**, 1–18.

Henares, S., **Caracciolo, L.**, **Cultrone, G.**, **Fernández, J.** and **Viseras, C.** (2014) The role of diagenesis and depositional facies on pore system evolution in a Triassic outcrop analogue (SE Spain). *Mar. Petrol. Geol.*, **51**, 136–151.

Henares, S., **Arribas, J.**, **Cultrone, G.** and **Viseras, C.** (2016a) Muddy and dolomitic rip-up clasts in Triassic fluvial sandstones: origin and impact on potential reservoir properties (Argana Basin, Morocco). *Sed. Geol.*, **339**, 218–233.

Henares, S., **Caracciolo, L.**, **Viseras, C.**, **Fernández, J.** and **Yeste, L.M.** (2016b) Diagenetic constraints on heterogeneous reservoir quality assessment: a Triassic outcrop analogue of meandering fluvial reservoirs. *AAPG Bull.*, **100**, 1377–1398.

Hubbard, S.M., **Smith, D.G.**, **Nielsen, H.**, **Leckie, D.A.**, **Fustic, M.**, **Spencer, R.J.** and **Bloom, L.** (2011) Seismic geomorphology and sedimentology of a tidally influenced river deposit, Lower Cretaceous Athabasca oil sands, Alberta, Canada. *AAPG Bull.*, **95**, 1123–1145.

Ielpi, A. and **Ghinassi, M.** (2014) Planform architecture, stratigraphic signature and morphodynamics of an exhumed Jurassic meander plain (Scalby Formation, Yorkshire, UK). *Sedimentology*, **61**, 1923–1960.

Ielpi, A., **Fralick, P.**, **Ventra, D.**, **Ghinassi, M.**, **Lebeau, L.E.**, **Marconato, A.**, **Meek, R.** and **Rainbird, R.** (2018) Fluvial floodplains prior to greening of the continents: stratigraphic record, geodynamic setting and modern analogues. *Sed. Geol.*, **372**, 140–172.

Jenson, M.A. and **Pedersen, G.K.** (2010) Architecture of vertically stacked fluvial deposits, Atane formation, Cretaceous, Nuussuaq, centralWest Greenland. *Sedimentology*, **57**, 1280–1314.

Jordan, D.W. and **Pryor, W.A.** (1992) Hierarchical levels of heterogeneity in a Mississippi River meander belt and application to reservoir systems. *AAPG Bull.*, **76**, 1601–1624.

Keeton, G.I., **Pranter, M.J.**, **Cole, R.D.** and **Gustason, E.R.** (2015) Stratigraphic architecture of fluvial deposits from borehole images, spectral-gamma-ray response, and outcrop analogs, Piceance Basin, Colorado. *AAPG Bull.*, **99**, 1929–1956.

Kokureck, G., **Knigth, J.** and **Havholm, K.** (1991) Outcrop of semi-regional three-dimensional architecture and reconstruction of a portion of the eolian Page Sandstone (Jurassic). In: *The Three-Dimensional Facies Architecture of Terrigenous Clastic Sediments and its Implications for Hydrocarbon Discovery and Recovery* (Eds Miall, A.D. and Tyler, N.), SEPM Concepts in Sedimentology and Paleontology, Tulsa, **3**, 25–43.

Kraus, M.J. and **Aslan, A.** (1999) Paleosol sequences in floodplain environments: a hierarchical approach. In: *Palaeoweathering, Palaeosurfaces and Related Continental Deposits* (Ed. Thiry, M.), IAS Special Publication, **27**, 303–321.

Lai, J., **Wang, G.**, **Wang, S.**, **Cao, J.**, **Li, M.**, **Pang, X.**, **Han, C.**, **Fan, X.**, **Yang, L.**, **He, Z.** and **Qin, Z.** (2018) A review on the applications of image logs in structural analysis and sedimentary characterization. *Mar. Petrol. Geol.*, **95**, 139–166.

Legarreta, L., **Uliana, M.A.**, **Larotonda, C.A.** and **Meconi, G.R.** (1993) Approaches to nonmarine sequence

stratigraphy-theoretical models and examples from Argentine basins. *Collection Colloques et Seminaires – Institut Francais du Petrole*, **51**, 125–144.

Li, J. and **Bristow, C.** (2015) Crevasse splay morphodynamics in a dryland river terminus: Río Colorado in Salar de Uyuni Bolivia. *Quatern. Int.*, **377**, 71–82.

Li, J., **Donselaar, M.**, **Enayat Hosseini Aria, S.**, **Koenders, R.** and **Oyen, A.M.** (2014) Landsat imagery-based visualization of the geomorphological development at the terminus of a dryland river system. *Quatern. Int.*, **352**, 100–110.

McGowen, J.H. and **Garner, L.E.** (1970) Physiographic features and stratification types of coarse-grained point bars: modern and ancient examples. *Sedimentology*, **14**, 77–111.

Miall, A.D. (1990) *Principles of Sedimentary Basin analysis*, 2nd edn. Springer Verlag Inc., New York, 668 p.

Miall, A.D. (1996) *The Geology of Fluvial Deposits*. Springer-Verlag, Heidelberg, 582 pp.

Mjøs, R., **Walderhaug, O.** and **Prestholm, E.** (1993) Crevasse splay sandstone geometries in the Middle Jurassic Ravenscar Group of Yorkshire, UK. In: *Alluvial Sedimentation* (Eds Marzo, M. and Puigdefábregas, C.), IAS Special Publication, **17**, 167–184.

Moscariello, A. (2009) Unraveling reservoir architecture of complex low net:gross Red-Bed fluvial sequence using palaeosoils and chemostratigraphy. *AAPG Cape Town, Search and Discovery Article* #50173.

Myers, K.J. and **Bristow, C.S.** (1989) Detailed sedimentology and gamma-ray log chracateristics of a Namurian deltaic succession II: gamma-ray logging. In: *Deltas Sites and Traps for Fossil Fuels* (Eds Whateley, M.K.G. and Pickering, K.T.), Geological Society Special Publication, **41**, 81–88.

Nanson, G.C. and **Page, K.** (1983) Lateral accretion of fine-grained concave benches associated with meandering rivers. In: *Modern and Ancient Fluvial Systems* (Eds Collinson, J.D. and Lewin, J.), IAS Special Publication, **6**, 133–143.

Nemec, W. and **Postma, G.** (1993) Quaternary alluvial fans in southwestern Crete: sedimentation processes and geomorphic evolution. In: *Alluvial Sedimentation* (Eds Marzo, M. and Puigdefabregas, C.), IAS Special Publication, **17**, 235–276.

Owen, G. and **Santos, M.G.** (2014) Soft-sediment deformation in a pre-vegetation river system: the Neoproterozoic Torridonian of NWScotland. *Proc. Geol. Assoc.*, **125**, 511–523.

Pizzuto, J.E. (1987) Sediment diffusion during overbank flows. *Sedimentology*, **34**, 301–317. https://doi.org/10.1111/j.1365-3091.1987.tb00779.x

Pranter, M.J., **Vargas, M.F.** and **Davis, T.L.** (2008) Characterization and 3D reservoir modelling of fluvial sandstones of the Williams Fork Formation, Rulison Field, Piceance Basin, Colorado, USA. *J. Geophys. Eng.*, **5**, 158–172.

Pranter, M.J., **Cole, R.D.**, **Panjaitan, H.** and **Sommer, N.K.** (2009) Sandstone-body dimensions in a lower coastal-plain depositional setting: Lower Williams fork formation, coal Canyon, Piceance Basin, Colorado. *AAPG Bull.*, **93**, 1379–1401.

Pranter, M.J., **Hewlett, A.C.**, **Cole, R.D.**, **Wang, H.** and **Gilman, J.R.** (2014) Fluvial architecture and connectivity of the Williams Fork Formation: use of outcrop analogues for stratigraphic characterisation and reservoir modelling. In: *Sediment-body Geometry and Heterogeneity: Analogue Studies for Modelling the Subsurface* (Eds Good, T., Howell, J. and Martinius, A.W.), Geological Society, London, Special Publications, **387**, 57–83.

Retallack, G.J. (2001) *Soils of the Past: An Introduction to Paleopedology*, 2nd edn. Blackwell Science, Oxford, 404 pp.

Retallack, G.J. and **Dilcher, D.L.** (2012) Outcrop versus core and geophysical log interpretation of mid-Cretaceous palaeosols from the Dakota Formation of Kansas. *Palaeogeogr. Palaeoclimatol. Palaeoecol.*, **329–330**, 47–63.

Rider, M. and **Kennedy, M.** (2011) *The Geological Interpretation of Well Logs*, 3rd edn. Rider-French Consultig, pp. 432. ISBN 978-0-9541906-8-2.

Rossi, C., **Kälin, O.**, **Arribas, J.** and **Tortosa, A.** (2002) Diagenesis, provenance and reservoir quality of Triassic TAGI sandstones from Ourhoud field, Berkine (Ghadames) Basin, Algeria. *Mar. Petrol. Geol.*, **19**, 117–142.

Rossetti, D.F. and **Santos, A.E.** (2003) Events of sediment deformation and mass failure in Upper Cretaceous estuarine deposits (Cametá Basin, northern Brazil) as evidence for seismic activity. *Sed. Geol.*, **161**, 107–130. https://doi.org/10.1016/S0037-0738(02)00398-6

Sánchez-Moya, Y., **Arribas, J.**, **Gómez-Gras, D.**, **Marzo, M.**, **Pérez-Arlucea, M.** and **Sopeña, A.** (2004) Inicio del rifting. El comienzo del relleno continental. In: *Geología de España* (Ed. Vera, J.A.), pp. 485–487. SGE-IGME, Madrid.

Scott, A., **Hurst, A.** and **Vigorito, M.** (2013) Outcrop-based reservoir characterisation of a kilometer-scale sand-injectite complex. *AAPG Bull.*, **97**, 309–343.

Selley, R.C. (2004) *Ancient Sedimentary Environments and Their Sub-Surface Diagnosis*. Taylor and Francis Group, London, 297 pp.

Slatt, R.M. (2013) Stratigraphic Reservoir characterization for Petroleum Geologists, Geophysicists and Engineers, In: *Developments in Petroleum Science* (Ed Cubitt, J.) 2nd edn, pp. 688. Elsevier, Amsterdam, Netherlands. ISBN: 9780444563651

Slatt, R.M., **Buckner, N.**, **Abousleiman, Y.**, **Sierra, R.**, **Philp, P.**, **Miceli-Romero, A.**, **Portas, R.**, **O'Brien, N.**, **Tran, M.**, **Davis, R.** and **Wawrzyniec, T.** (2011) Outcrop/behind outcrop (quarry), multiscale characterisation of the Woodford Gas Shale, Oklahoma. In: *Shale Reservoirs—Giant Resources for the 21st Century* (Ed. Breyer, J.), AAPG Memoirs, **97**, 1–21.

Soil Survey Staff (1998) *Key to Soil Taxonomy*, 8th edn. United States Department of Agriculture, Natural Resources Conservation Service, Washington, DC, 328 pp.

Thomas, R.G., **Smith, D.G.**, **Wood, J.M.**, **Visser, J.**, **Calverley-Range, E.A.** and **Koster, E.H.** (1987) Inclined heterolithic stratification-terminology, description, interpretation and significance. *Sed. Geol.*, **53**, 123–179.

Tyler, N. and **Finley, R.J.** (1991) Architectural controls on the recovery of hydrocarbons from sandstone reservoirs. In: *The Three-Dimensional Facies Architecture of Terrigenous Clastic Sediments and its Implications for Hydrocarbon Discovery and Recovery* (Eds Miall, A.D. and Tyler, N.), SEPM Concepts in Sedimentology and Paleontology, Tulsa, **3**, 1–5.

Van Toorenenburg, K.A., **Donselaar, M.E.**, **Noordijk, N.A.** and **Weltje, G.J.** (2016) On the origin of crevasse-splay amalgamation in the Huesca fluvial fan (Ebro Basin, Spain): implications for connectivity in low net-to-gross fluvial deposits. *Sed. Geol.*, **343**, 156–164.

Varela, A.N., **Veiga, G.D.** and **Poiré, D.G.** (2012) Sequence stratigraphic analysis of Cenomanian greenhouse palaeosols: a case study from southern Patagonia, Argentina. *Sed. Geol.*, **271–272**, 67–82.

Varela, A.N., **Yeste, L.M.**, **Viseras, C.** and **García-García, F.** (2019) Implications of palaeosols in low net-to-gross

fluvial architecture reconstruction: reservoirs analogues from Patagonia and Spain. *34th IAS Meeting of Sedimentology*, 10–13 Sep 2019, Rome, Italy.

Viseras, C., **Fernández, J.** and **Henares, S.** (2011) Facies architecture in outcropping analogues for the TAGI Reservoir. Exploratory Interest. *AAPG International Conference and Exhibition, Search and Discovery Article, #90135, Milan (Italy).*

Viseras, C., **Henares, S.**, **Yeste, L.M.** and **García-García, F.** (2018) Reconstructing the architecture of ancient meander belts by compiling outcrop and subsurface data: a Triassic example. In: *Fluvial Meanders and Their Sedimentary Products in the Rock Record* (Eds Ghinassi, M., Colombera, L., Mountney, N.P. and Reesink, A.J.H.), IAS Special Publication, **48**, 419–444.

Weber, K.J. (1986) How heterogeneity affects oil recovery. In: *Reservoir Characterization* (Eds Lake, L.W. and Carroll, N.B. Jr), pp. 545–560. Academy Press, Orlando, FL.

Wizevich, M.C. (1991) Photomosaics of outcrops: useful photographic techniques. In: *The Three-Dimensional Facies Architecture of Terrigenous Clastic Sediments and its Implications for Hydrocarbon Discovery and Recovery* (Eds Miall, A.D. and Tyler, N.), SEPM Concepts in Sedimentology and Paleontology, Tulsa, **3**, 22–24.

Xu, C., **Cronin, T.P.**, **McGinness, T.E.** and **Steer, B.** (2009) Middle Atokan sediment gravity flows in the Red Oak field, Arkoma Basin, Oklahoma: a sedimentary analysis using electrical borehole images and wireline logs. *AAPG Bull.*, **93**, 1–29.

Yeste, L.M., **Henares, S.**, **McDougall, N.**, **García-García, F.** and **Viseras, C.** (2018) Towards the multi-scale characterization of braided fluvial geobodies from outcrop, core, georradar and well logs data. In: *River to Reservoir: Geoscience to Engineering* (Eds Corbett, P., Owen, A., Hartley, A., Pla-Pueyo, S., Barreto, D., Hackney, C. and Kape, S.), GSL Special Publication, **488**. https://doi.org/10.1144/sp488.3

Yeste, L.M., **Palomino, R.**, **McDougall, N.**, **Viseras, C.**, **Varela, A.N.** and **García-García, F.** (2019) Towards Geocellular modelling of highly heterogeneous reservoirs. A Triassic example. *34th IAS Meeting of Sedimentology*, 10–13 Sep 2019, Rome, Italy.

Yoshida, S., **Jackson, M.D.**, **Johnson, H.D.**, **Muggeridge, A.H.** and **Martinius, A.W.** (2001) Outcrop studies of tidal sandstones for reservoir characterization (Lower Cretaceous Vectis Formation, Isle of Wight, Southern England). In: *Sedimentary Environments Offshore Norway – Palaeozoic to Recent* (Eds Martinsen, O.J. and Dreyer, T.), Norwegian Petroleum Society Special Publication, **10**, 233–257.

Manuscript received 3 June 2019; revision accepted 8 April 2020